



## Supplementary Materials for

### **Sequence-dependent activity and compartmentalization of foreign DNA in a eukaryotic nucleus**

Léa Meneu *et al.*

Corresponding authors: Jacques Serizay, jacques.serizay@pasteur.fr; Julien Mozziconacci, julien.mozziconacci@mnhn.fr;  
Romain Koszul, romain.koszul@pasteur.fr

*Science* **387**, eadm9466 (2025)  
DOI: 10.1126/science.adm9466

#### **The PDF file includes:**

Supplementary Text  
Figs. S1 to S11  
Tables S1 to S5  
References

#### **Other Supplementary Material for this manuscript includes the following:**

MDAR Reproducibility Checklist

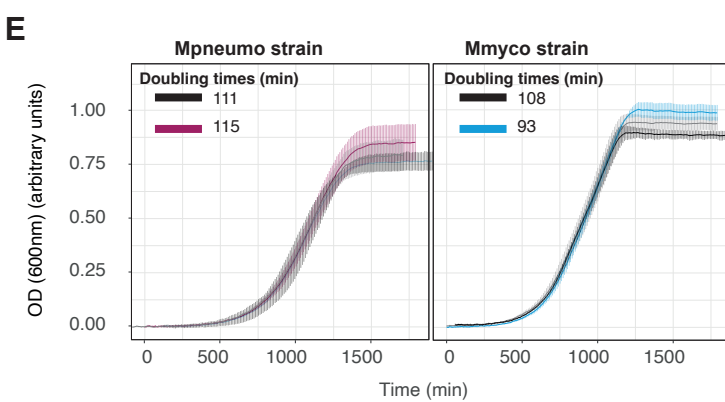
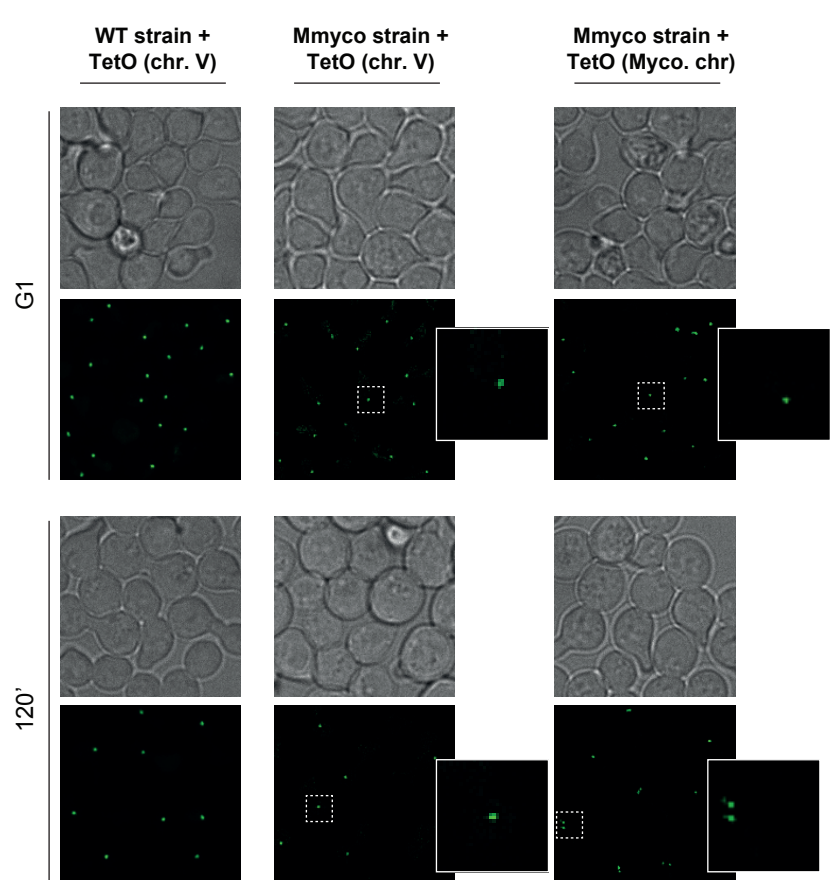
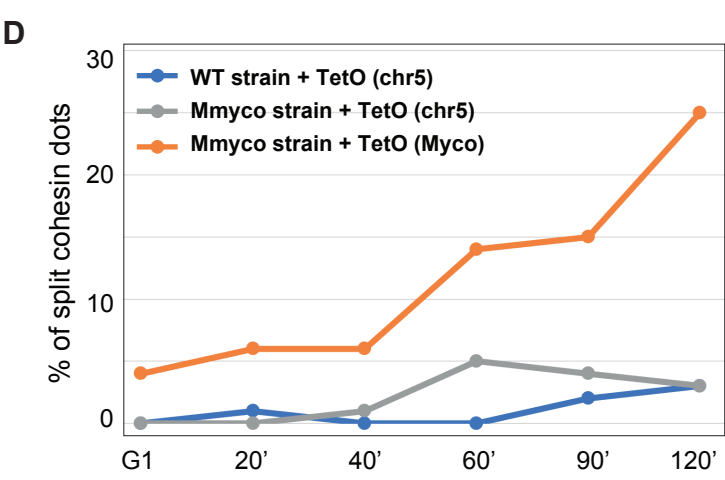
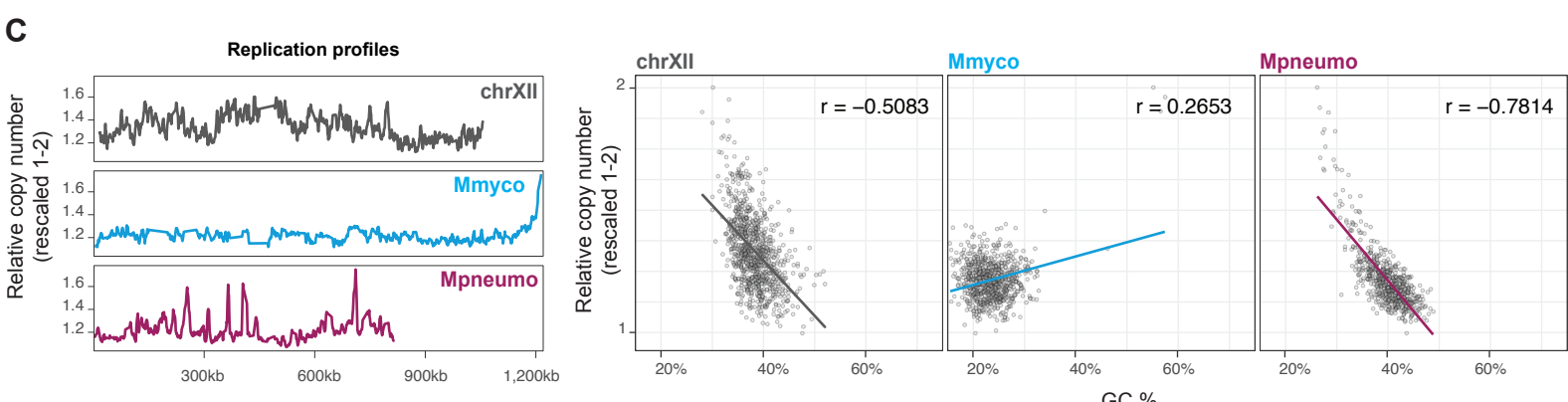
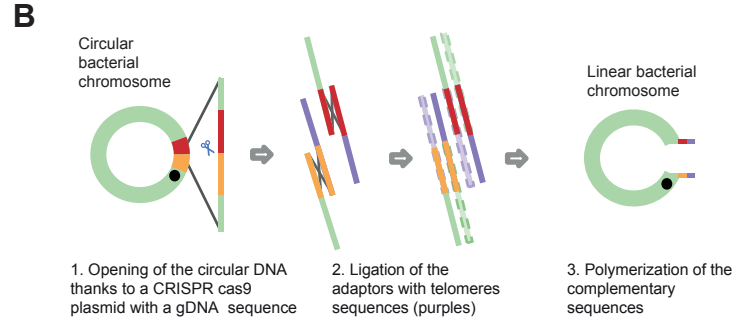
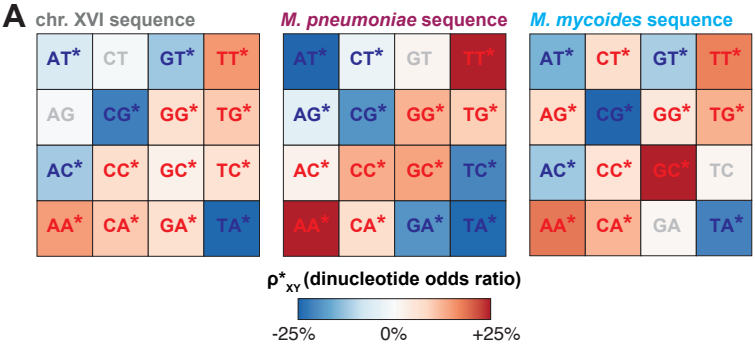
## Supplementary Text

### Replication and pairing of artificial chromosomes

DNA sequence composition and chromatin factors, including nucleosomes, are essential drivers of the replication timing, prompting us to investigate how this timing is established in Y and U chromatin (92).

In yeast, replication initiates at the level of discrete, small autonomous replication sequences (ARS) positioned along all chromosomes. To investigate the replication timing profile of both bacterial chromosomes, which did not spontaneously evolve to contain these sequences, we used Repliscore (Methods)(93). Mpneumo Repliscore profile exhibits DNA copy number variation comparable to that observed along chrXII, indicative of early or mid-S phase firing of multiple replication origins (Fig. S1C). This copy number is anti-correlated with GC%, consistent with AT-rich regions replicating earlier. In contrast, DNA copy number variation along Mmyco unveils the early firing of only the centromere-proximal ARS which was artificially integrated during chromosome assembly (Fig. S1C). The average copy number of the rest of the Mmyco chromosome appears flat and is not anti-correlated with the GC%. Thus, the replication of U-type chromatin occurs later during the S phase despite its AT-rich sequence composition. These observations confirm the predominant role of chromatin composition in the replication timing, and indicate a heterochromatin-like effect exerted by the U-type chromatin. This pattern is reminiscent of the random and late-replication pattern displayed by the human inactive chromosome X (94).

DNA replication and SCC are closely related as cohesion is established during S phase through entrapment of sister DNA molecules by cohesin rings as the replication fork progresses (20). We therefore investigated SCC by performing image analysis of chromosome pairing (Methods; Fig. S1D). Despite the strong enrichment in Scc1 deposition, SCC in Mmyco appears significantly reduced, in agreement with the flat replication pattern suggesting a late and random initiation of the replication process. On the other hand, the endogenous yeast chromosomes in Mmyco strain did not display a significant decrease in SCC (Fig. S1D), despite the apparent loss of cohesin at centromeres.



**F**

Percent (P) chromosome-carrying cells

	After 10 doublings selective	After g doublings nonselective	Segregation rate	
	$P_1$	$g$	$P_2$	$m$
Mmyco.	91.07	11.72	74.8	1.7
Mpneumo.	76.8	11.70	50.7	3.5

Fig. S1

**Fig. S1. Characterization of Mpneumo and Mmyco strains metabolism.**

**A**, Dinucleotide over-representation ( $\rho^*(XY)$ ) in yeast chromosome XVI, Mpneumo and Mmyco chromosomes.

**B**, Schematic representation of the CRISPR-Cas9 strategy applied to linearize and telomerize the circular bacterial genomes.

**C**, MFA (replication profile) analysis of a representative WT yeast chromosome, and of Mmcyo and Mpneumo chromosomes.

**D**, Cohesin split dot assays in WT strain (TetO array in chr. V), or in Myco strain (TetO array in chr. V or Myco. chromosome). Top left: % of split cohesin dots in each strain upon G1-release; bottom left: cell ploidy upon G1-release; right: representative cohesin immunofluorescence imaging in each strain following G1-release.

**E**, Growth curves of WT, Mpneumo and Mmyco strains. For each strain, 3 independent cultures were performed. A pRS413 centromeric plasmid similar to the one onto which bacterial chromosomes were originally cloned is included in the WT strain as a control.

**F**, The chromosome stability and the segregation rate were measured as described in (67) (**Methods**). Yeast strains used are RSG\_Y712 (Mmyco linear) and RSG\_Y960 (Mpneumo linear). P1: % of bacterial chromosome-carrying cells in selective media. g: number of doubling. P2: of bacterial chromosome-carrying cells after 12 generations in non-selective media. m: segregation rate, i.e. % of plasmid-free segregants appearing in the final population after a single doubling.

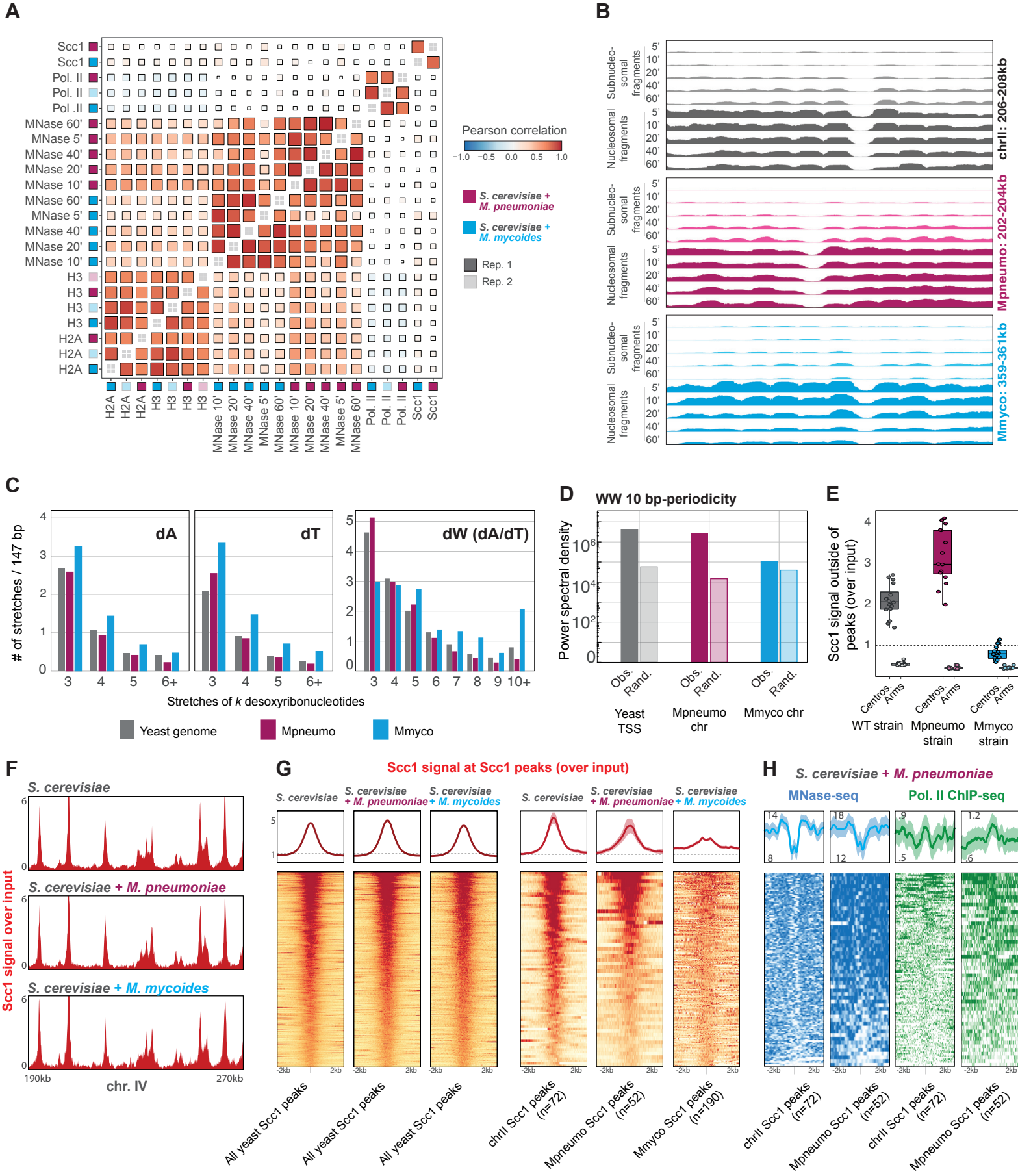


Fig. S2

**Fig. S2. Replication of bacterial genomes in yeast.**

- A**, Pearson correlation between replicates of MNase and ChIP experiments. Bin size: 100bp.
- B**, Coverage of sub-nucleosomal (smaller than 130bp) or nucleosomal (between 130 and 165bp) fragments over 2kb-long genomic loci from chr. II, Mpneumo and Mmyco chromosomes, over an MNase digestion timecourse. All the tracks are displayed at the same scale (0-20 CPM).
- C**, Number of poly-dA, poly-dT and poly-dW (dA/dT) stretches of various lengths in the yeast genome and over the Mpneumo and Mmyco chromosomes. Stretch numbers are scaled to 147bp.
- D**, Power spectral density (PSD) of WW 10-bp periodicity, in 300bp-long sequences centered over yeast TSSs or along the Mpneumo or Mmyco chromosomes. Random sequences were generated by shuffling actual sequences while preserving dinucleotide frequency.
- E**, Cohesin (Scc1) enrichment over yeast centromeres and yeast arms in WT, Mpneumo and Mmyco strains. Scc1 signal over arms was calculated outside of any Scc1 peak.
- F**, Representative 80kb window of Scc1 ChIP-seq deposition signal over yeast chr. IV in the WT, Mpneumo, and Mmyco strains.
- G**, Aggregated profile of Scc1 deposition centered at Scc1 peaks (+/- 2kb) called over all endogenous (left panels) or only chr. II (right panels) yeast chromosomes in the WT, Mpneumo and Mmyco strains.
- H**, Aggregated profile of MNase-seq (blue) or Pol. II (green) deposition centered at Scc1 peaks (+/- 2kb) called over the yeast chromosome II (left) or the Mpneumo chromosome (right).

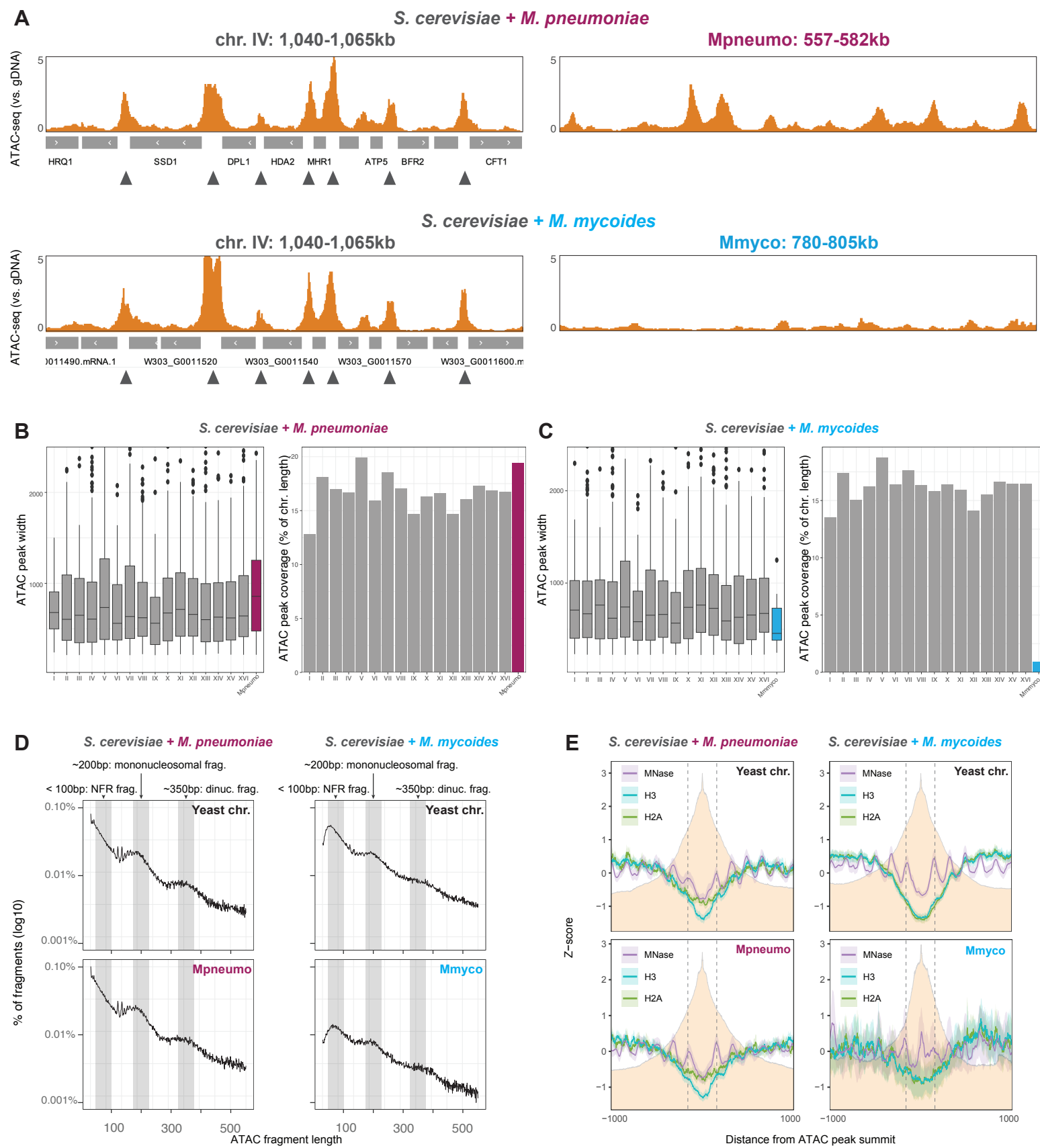


Fig. S3

**Fig. S3. Chromatin accessibility of bacterial chromosomes in yeast.**

**A**, ATAC-seq profiles (chromatin/gDNA) obtained in the Mpneumo strain (*S. cerevisiae* + *M. pneumoniae*) and Mmyco strain (*S. cerevisiae* + *M. mycoides*) (10kb-long genomic windows over the chromosome IV, Mpneumo and Mmyco chromosomes).

**B-C**, ATAC-seq analysis comparing *S. cerevisiae* with *M. pneumoniae* (**B**) or with *M. mycoides* (**C**). Boxplots display ATAC peak widths and barplots summarize the total % of each chromosome covered by ATAC-seq peaks.

**D**, ATAC-seq fragment length distribution for *S. cerevisiae* combined with *M. pneumoniae* (left) and *M. mycoides* (right). ATAC-seq fragments obtained from nucleosome-free regions (<100 bp), mononucleosomal (~200 bp), and dinucleosomal (~350 bp) fragments are highlighted.

**E**, Average signal of nucleosome and histone ChIP-seq tracks over ATAC-seq peaks.

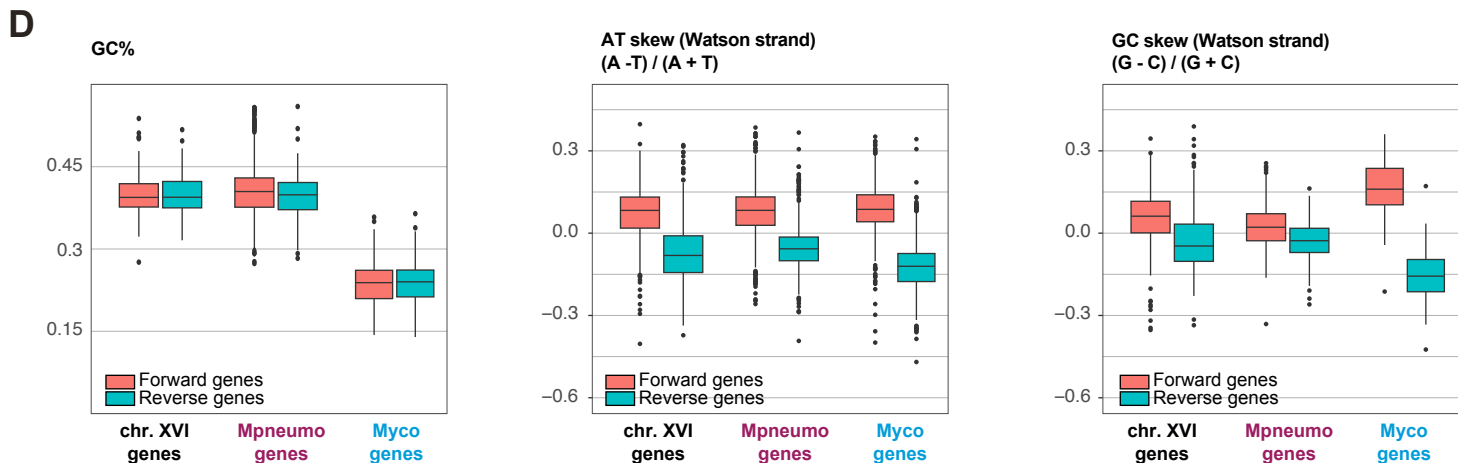
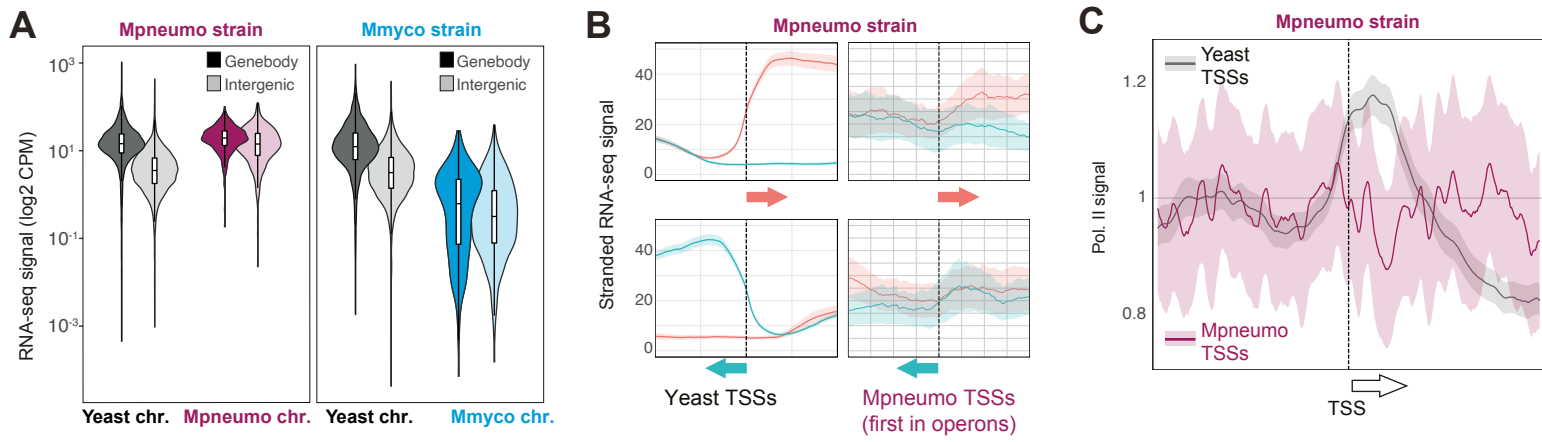


Fig. S4

**Fig. S4. Transcription orientation of bacterial chromosomes in yeast.**

**A**, RNA-seq average signal over yeast or bacterial gene bodies and intergenic regions, in Mpneumo and Mmyco strains. Scores were normalized by the length of each genomic feature (CPM: counts per million of sequenced fragments).

**B**, Stranded analysis of RNA-seq data in Pneumo. strain. Pile-up of 1kb windows centered on transcription start sites (TSS) of genes either in the forward (Top) or reverse (Bottom) orientation. Left: endogenous yeast genes. Right: TSS of the first gene of annotated operons along the *M. pneumoniae* sequence.

**C**, Pol. II ChIP-seq coverage analysis in Pneumo strain. Pile-up of 2kb windows centered on transcription start sites (TSS). Grey: endogenous yeast genes. Purple: TSS of the first gene of annotated operons along the *M. pneumoniae* sequence.

**D**, GC content (left), average AT (middle) and GC (right) skews (computed on Watson strand) over yeast, Myco and Mpneumo forward or reverse genes.

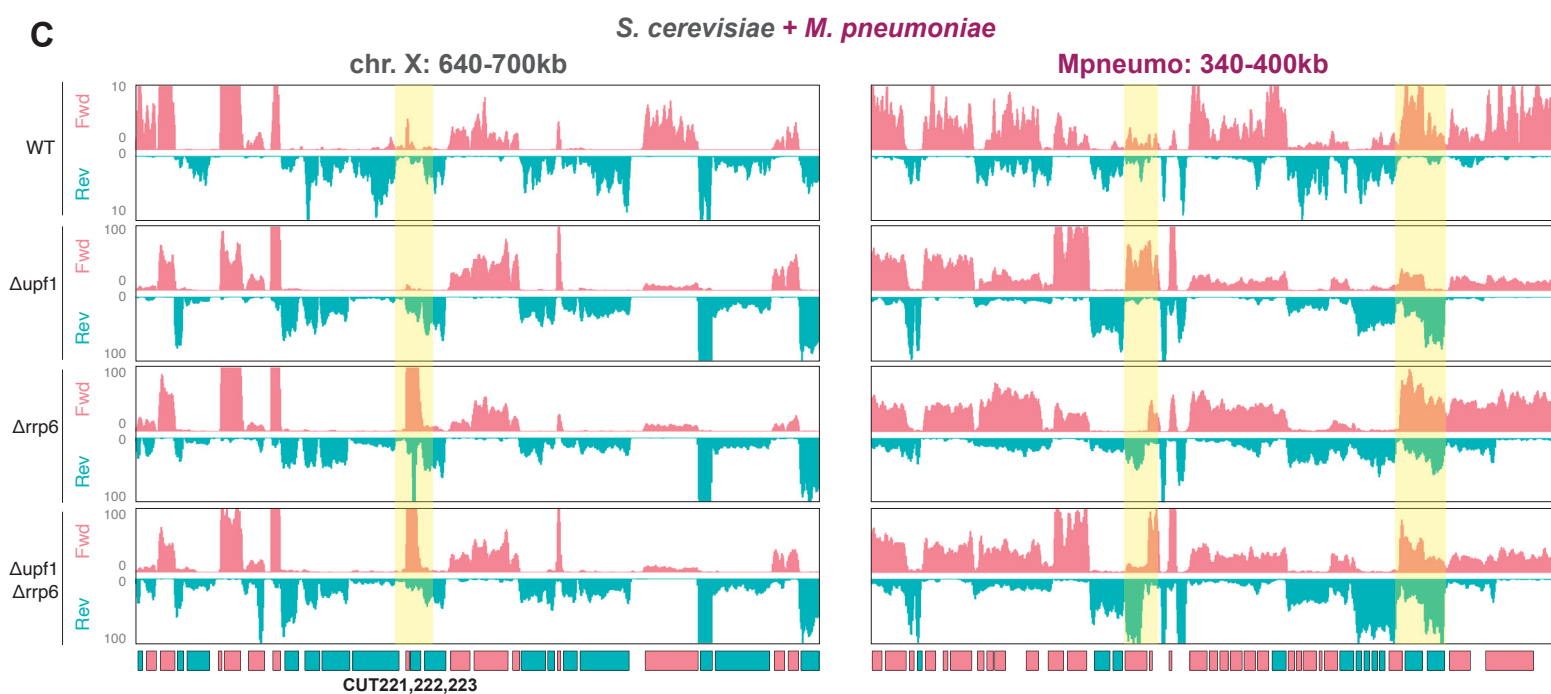
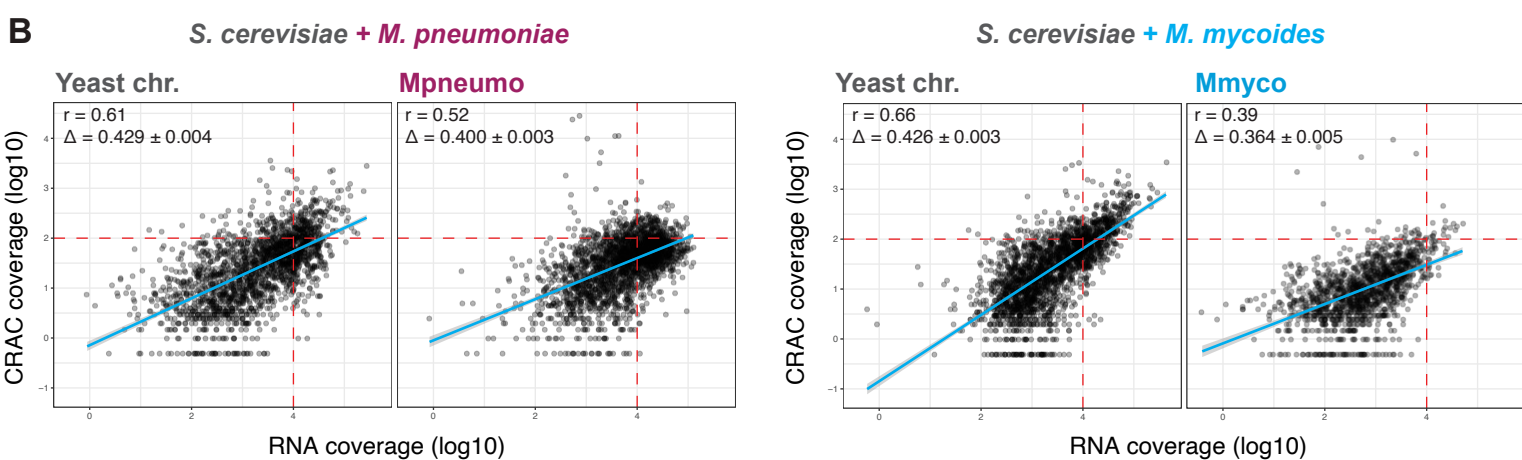
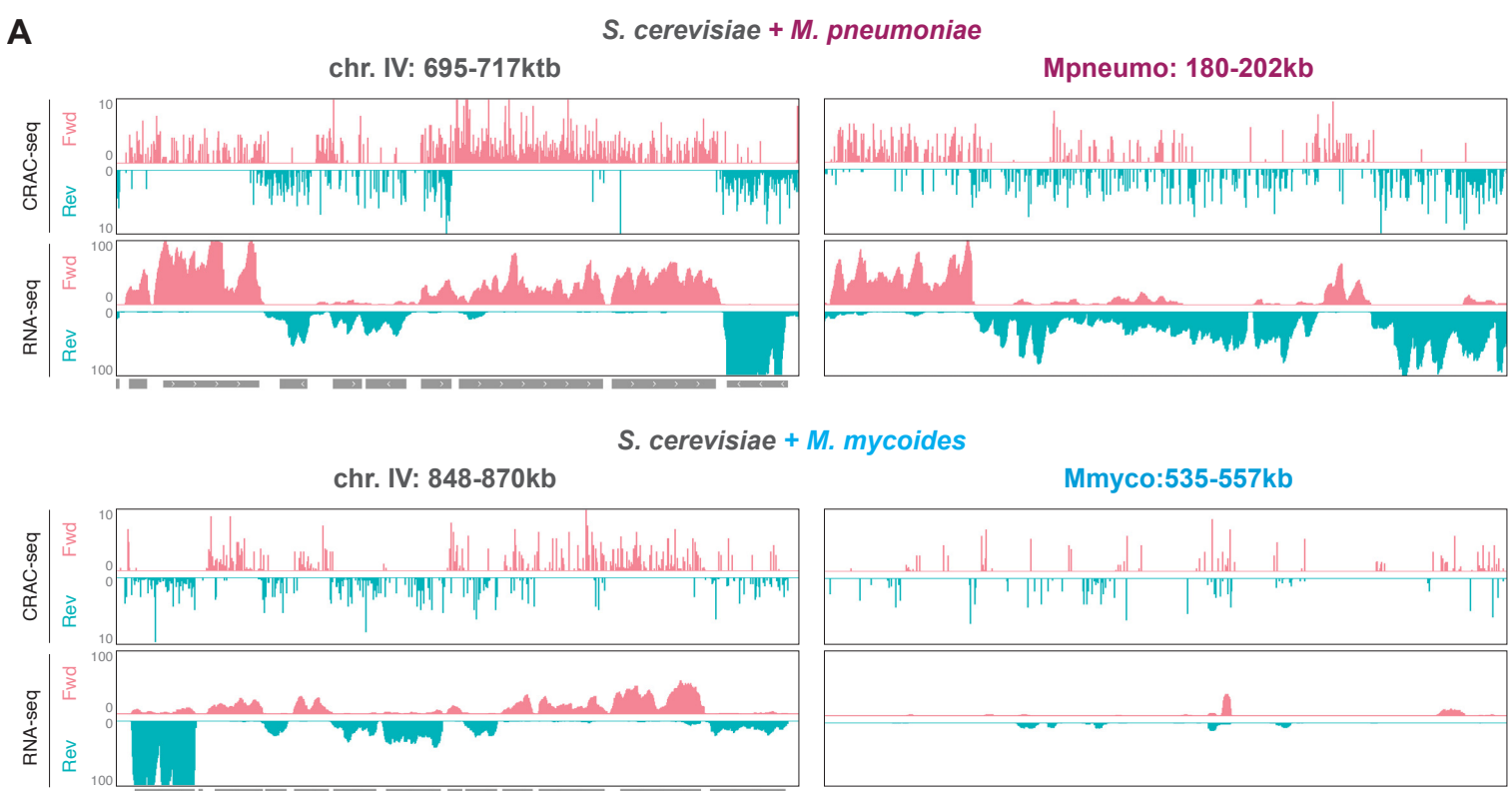
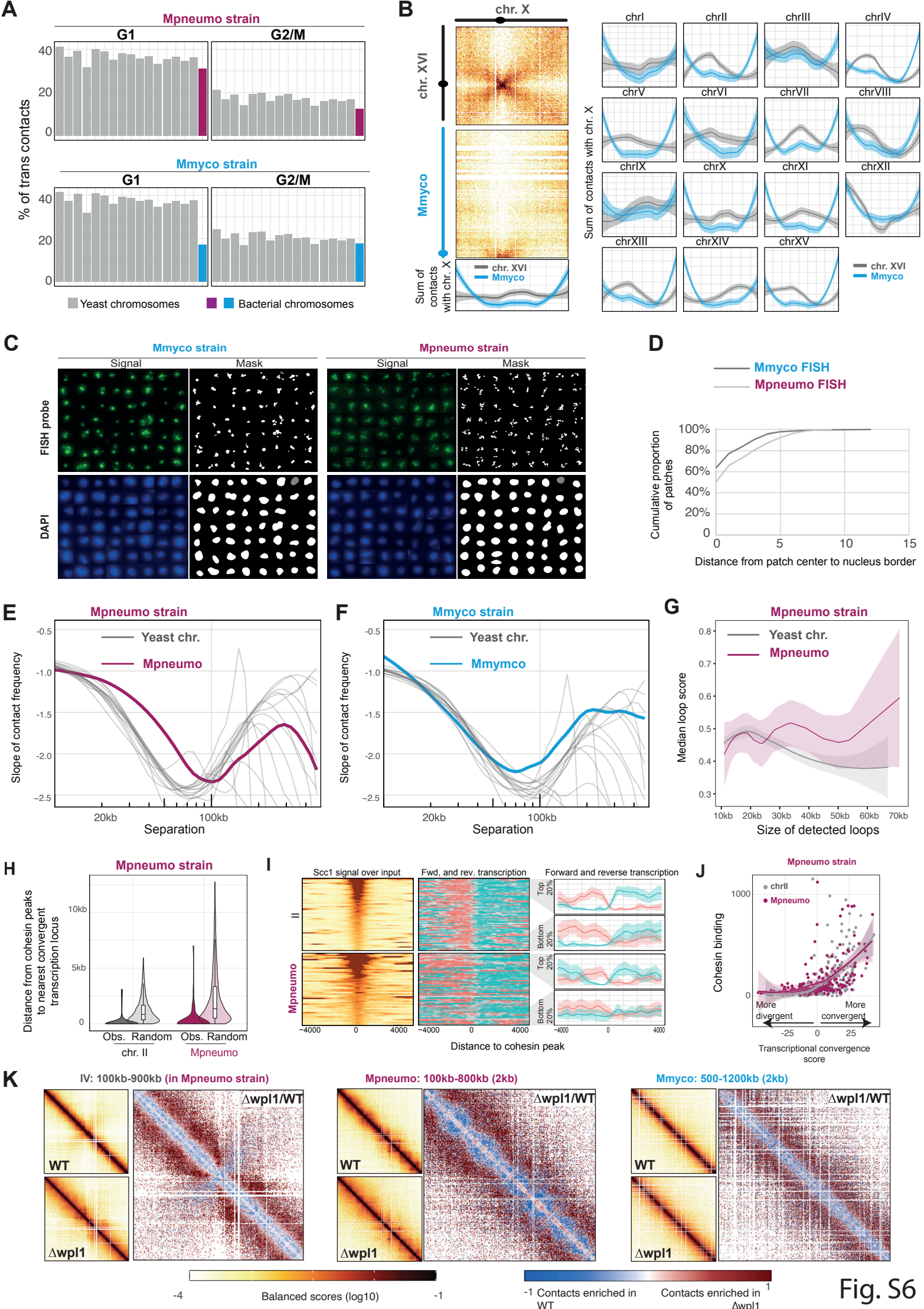


Fig. S5

**Fig. S5. Nascent transcription of bacterial chromosomes in yeast.**

- A.** Stranded CRAC-seq and RNA-seq profiles along chr. IV, Mpneumo and Mmyco chromosomes (CPM). Forward transcription profiles are shown in pink, and reverse transcription profiles are shown in turquoise.
- B,** Relationship between CRAC and RNA coverage, in *S. cerevisiae* strains with *M. pneumoniae* (left) or with *M. mycoides* chromosome (right).
- C,** Stranded RNA-seq profiles of Mpneumo strains in WT or  $\Delta$ upf1,  $\Delta$ rrp6 and  $\Delta$ upf1/ $\Delta$ rrp6 mutants, along chr. X or Mpneumo chromosomes. Forward transcription profiles are shown in pink, and reverse transcription profiles are shown in turquoise.



**Fig. S6. Folding of exogenic bacterial sequences within the yeast nucleus.**

- A**, % of total trans-contacts made by endogenous yeast chromosomes, Mmyco (top) or Mpneumo (bottom) bacterial chromosomes, in G1 or G2/M.
- B**, Left: quantification of contacts between the entire Mmyco chromosome (blue) and endogenous yeast chr. X (grey). Right: similar analysis for the other 15 endogenous yeast chromosomes. Note the increase of Myco. contacts at yeast telomeres.
- C**, Series of nuclei from Mpneumo or Mmyco fixed cells labeled with DAPI and hybridized with a fluorescent probe generated from either purified Mmyco (left) or Mpneumo (right) chromosome (top row: probe signal; bottom row: DAPI signal).
- D**, Distance between the patch of fluorescent signal from either the Mmyco or Mpneumo chromosomes and the nucleus border. Note that the Mmyco patches are located closer to the nucleus border than Mpneumo ones.
- E, F**, Slope of distance-dependent contact frequency of endogenous yeast chromosomes and bacterial chromosomes in G2/M Mpneumo (**C**) and Mmyco (**D**) strains.
- G**, Distance-dependent loop scores (computed using Chromosight (84)) for loops along either endogenous (grey) or Mpneumo (purple) chromosomes.
- H**, Distance measured between cohesin peaks and their nearest convergent transcription locus, for peaks located in chr. II or in Mpneumo chromosome. Expected distances, measured after randomly shuffling the position of the cohesin peaks 100 times, are also shown.
- I**, Left: aggregated profile of Scc1 deposition centered at Scc1 peaks (+/- 4kb) called over chr. II (top) or Mpneumo (bottom), with peaks ordered by peak strength. Middle: corresponding stranded transcription tracks, colored according to their forward or reverse orientation. Right: for chr. II or Mpneumo chromosome, average forward and reverse transcription over the 20% strongest or 20% weakest Scc1 peaks.
- J**, Correlation between Scc1 (cohesin) binding and convergent transcription strength (see Methods) in chr. II and in Mpneumo chromosome.
- K**, For yeast chromosome IV, Mpneumo and Mmyco: Left, Hi-C contact maps of the endogenous yeast chromosome IV of the Mpneumo strain synchronized in G2/M in either WT and Wpl1 depleted cells ( $\Delta$ wpl1); Right, corresponding chr. IV ratio map ( $\Delta$ wpl1 over WT). Red (or blue) indicate enriched (or depleted) contacts in  $\Delta$ wpl1.

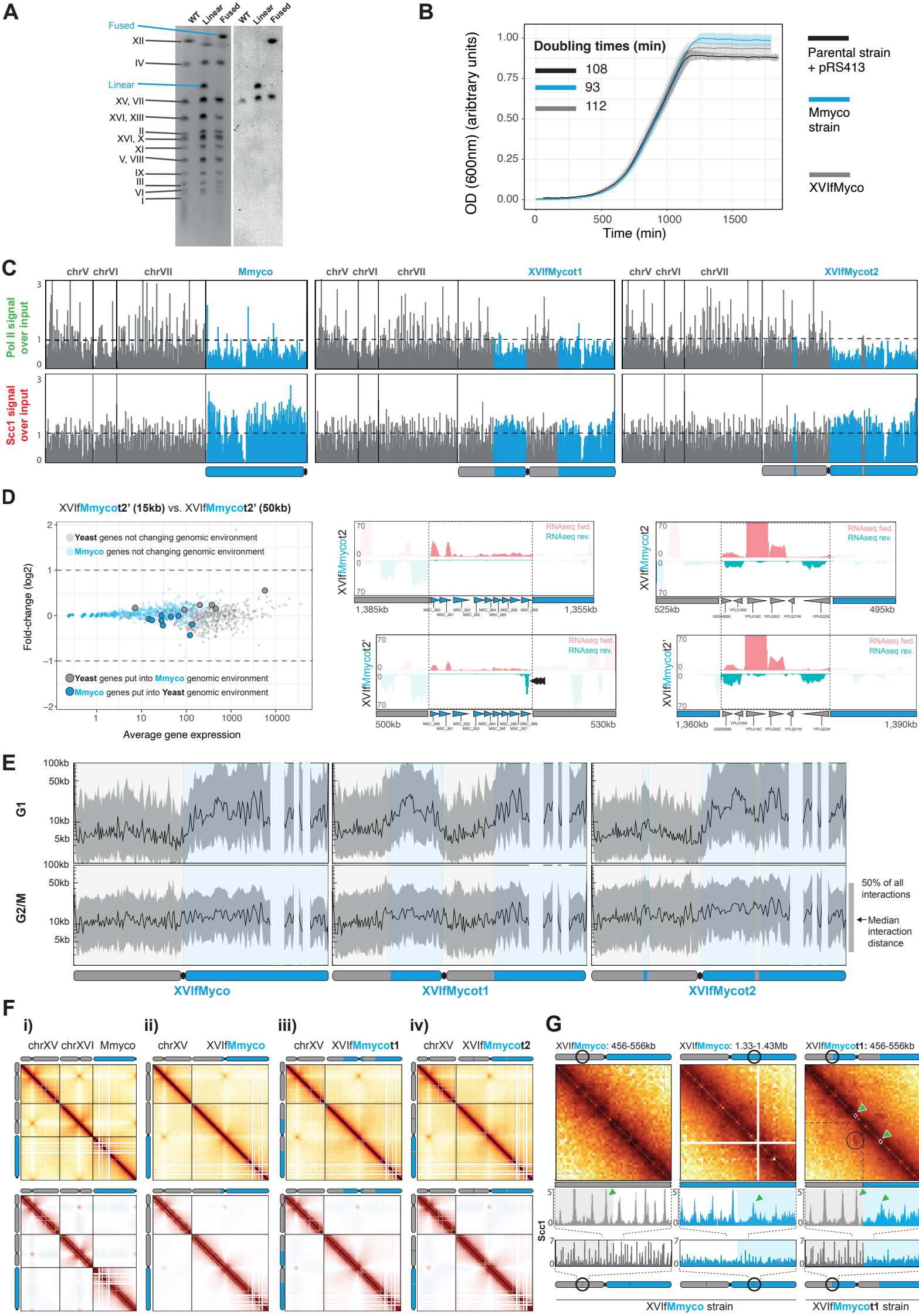


**Fig. S7. Compartmentalization of mosaic chromosomes composed of Y and U-type chromatin.**

**A**, Left: pulsed-field gel electrophoresis of chromosomes from yeast strains containing the Mmyco chromosome, either linear or fused with endogenous yeast chr. XVI (XVIIfMmyco strain). Right: Southern blot hybridization using a his-3 probe present on the Mmyco chromosome sequence (note that his-3 is also present on the endogenous chr. XV in the parental yeast strain).

**B**, Growth curves of WT, Mmyco and XVIIfMmyco strains.

**C**, Pol. II (top) and Scc1 (bottom) ChIP-seq deposition profiles along three representative yeast chromosomes and Mmyco chromosome (left) and mosaic chromosomes in XVIIfMmycot1 (center) and XVIIfMmycot2 (right) strains. Bin size: 10kb.

**D**, Expression fold-change (log2) against average expression, for genes located in yeast segments or Mmmcyo segments, between the XVIIfMmycot2 and the XVIIfMmycot2' strains. Genomic tracks illustrating stranded RNA-seq coverage over yeast (gray) and Mmmcyo (blue) genes, and their surrounding sequences (yeast: gray; Mmmcyo: blue).

**E**, Average distance of interaction along the fused and mosaic Mmyco chromosomes: XVIIfMmyco (left), XVIIfMmycot1 (center) and XVIIfMmycot2 (right). The shaded ribbon represents the interval between the 25% and 75% quantile of distance of interactions.

**F**, Top: G2/M Hi-C contact maps of chr. XV, XVI, and bacterial chromosomes in the Mmyco strain, and in its derivatives (i.e. the chr. XVI and Mmyco fusion, and the two strains with translocations resulting in alternating Y and U chromatin segments; Methods). Bottom: correlation contact matrices in wt and mosaic chromosomes strains. The color scales are the same as in Fig. 4B.

**G**, Hi-C contact maps in G2/M of 100 kb window of either the XVIIfMmyco (left and center) or XVIIfMmycot1 (right) chromosomes, centered on the translocation position of the XVIIfMmycot1 chromosome. In XVIIfMmycot1, this window is effectively centered at the junction between the yeast chr. XVI segment (upstream) and the Myco chromosome segment (downstream). The Scc1 deposition profile measured by ChIP-seq in each strain is shown underneath each contact map. Green arrows: cohesin peaks flanking the junction between the yeast and the Myco segments in the XVIIfMmycot1 chromosome..

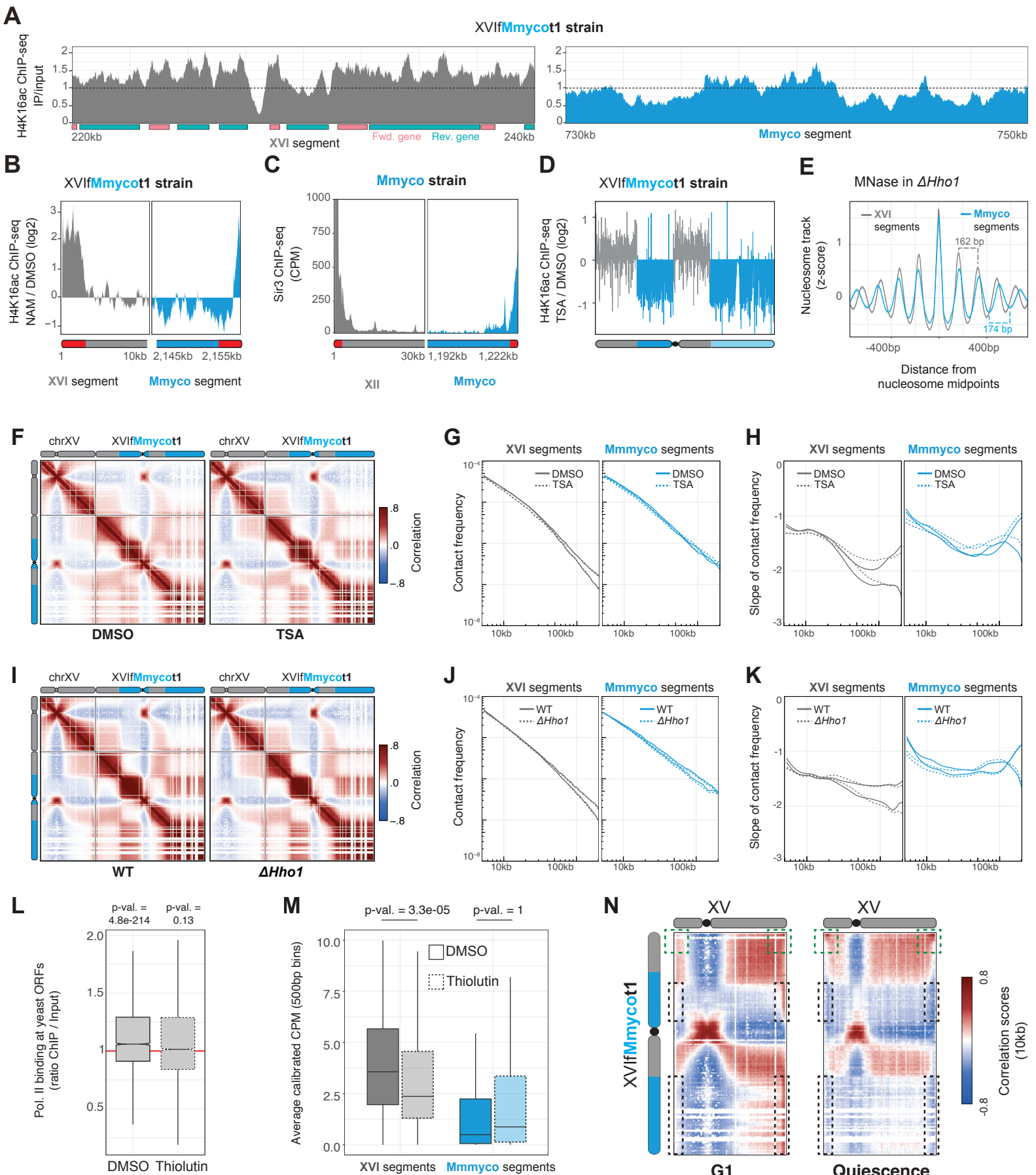


Fig. S8

**Fig. S8. Functional investigation of heterochromatinization mechanisms of U-type compartment.**

**A**, H4K16ac ChIP-seq profile (ratio IP/input) in the XVIIfMmycot1 strain, over a yeast chromosome segment (left) or a Myco chromosome segment (right).

**B**, Comparison of H4K16ac ChIP-seq profiles in the XVIIfMmycot1 strain, in cells treated by Nicotinamide (NAM) vs. DMSO (log2 scale). Telomeres and subtelomeric domains (2.5kb) are shown in red.

**C**, ChIP-seq profiles of Sir3 in the XVIIfMmycot1 strain. Telomeres and subtelomeric domains (2.5kb) are shown in red.

**D**, Comparison of H4K16ac ChIP-seq profiles in the XVIIfMmycot1 strain, in cells treated by Trichostatin A (TSA) vs. DMSO (log2 scale).

**E**, Nucleosome track over yeast (gray) or Mmyco nucleosomes (blue), in  $\Delta$ Hho1 yeast strain.

**F**, Correlation matrices of the contacts in chr. XV and XVIIfMmycot1 in G1, after the addition of DMSO (left) or TSA (right).

**G**, Contact frequency (p) as a function of genomic distance (s), for contacts in yeast segments (gray) or Mmmmyco segments (blue) of the chimeric chromosome XVIIfMmycot1, in G1 after the addition of DMSO (solid) or TSA (dotted).

**H**, Derivatives of curves from **F**.

**I**, Correlation matrices of the contacts in chr. XV and XVIIfMmycot1 in G1, after the addition of DMSO (left) or TSA (right).

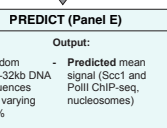
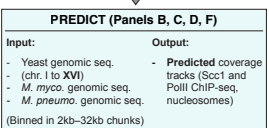
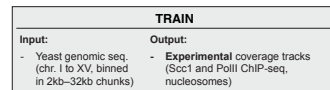
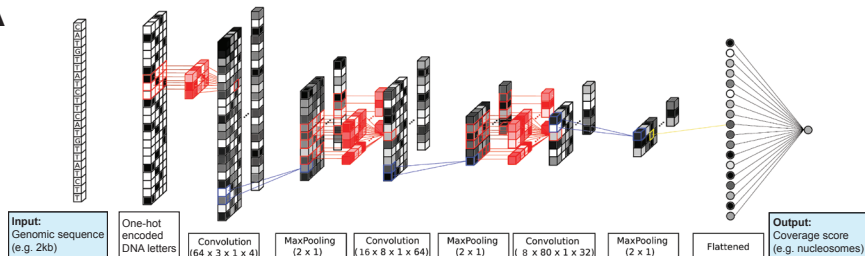
**J**, Contact frequency (p) as a function of genomic distance (s), for contacts in yeast segments (gray) or Mmmmyco segments (blue) of the chimeric chromosome XVIIfMmycot1, in WT (solid) or  $\Delta$ Hho1 mutant (dotted).

**K**, Derivatives of curves from **I**.

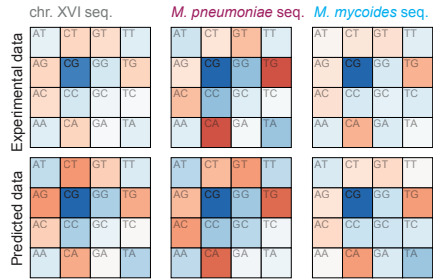
**L**, Average Pol. II ChIP-seq coverage (ratio IP/input) at every yeast ORF, in DMSO (solid) or after thiolutin treatment (dotted). P-values from one-sample two-tailed Student t-test.

**M**, Average RNA-seq coverage over 500bp bins from XVI (gray) or Mmmcyo (blue) segments, in DMSO (solid) or after thiolutin treatment (dotted). P-values from one-tailed Student's t-test.

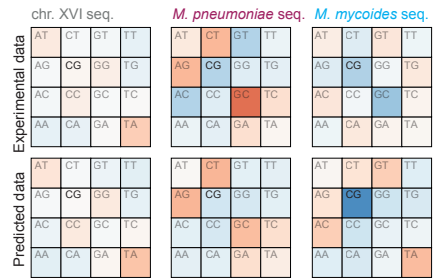
**N**, Correlation matrices of the trans-chromosomal contacts between chr. XV and XVIIfMmycot1 in G1, in G1 (left) or quiescence (right).

**A****B**

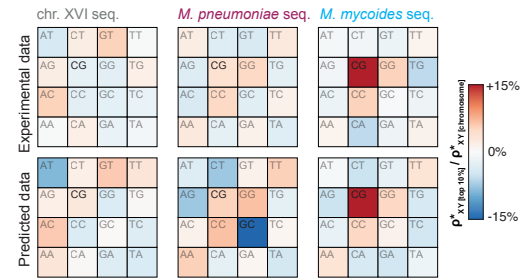
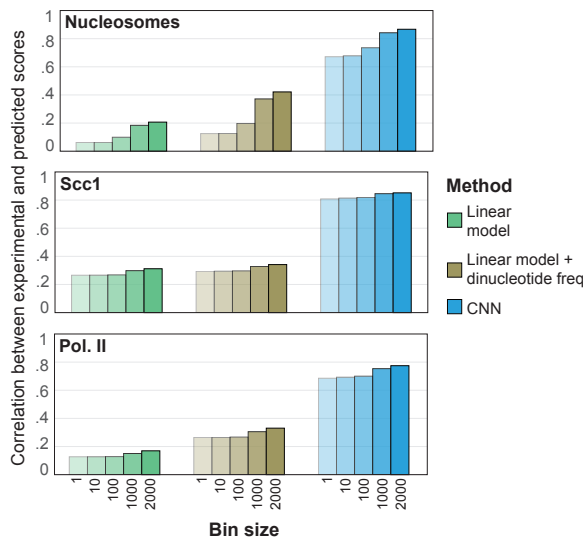
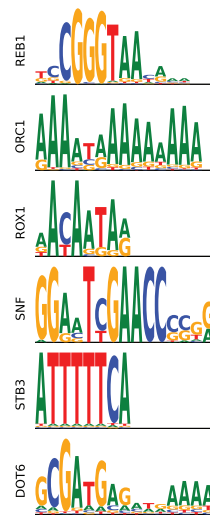
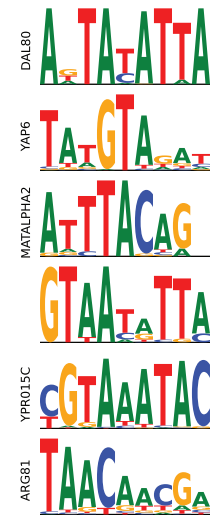
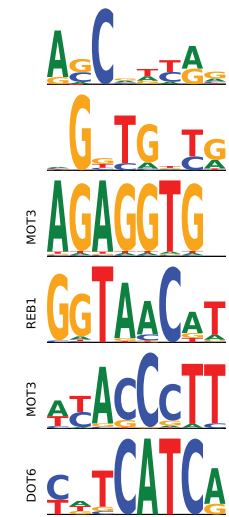
## Dinucleotide enrichment in top 10% nucleosome track bins



## Dinucleotide enrichment in top 10% Scc1 coverage bins



## Dinucleotide enrichment in top 10% PolII coverage bins

**C****Nucleosomes****ScC1****Pol. II****Fig. S9**

**Fig. S9. Sequence-based prediction of chromatin composition of exogenous bacterial chromosomes in yeast.**

**A**, Left: Schematic representation of the convolution neural network used in this study. The input of the network is a 2 to 30kb DNA sequence. The output is the corresponding value of the nucleosome, Scc1 or Pol. II signal. Details about the size of the input/output and the architecture used are discussed in the Material and Methods. Right: Overall training/prediction strategy.

We trained a CNN on sequences of chr. I-XV to predict (i) genome-wide nucleosome, Scc1 or Pol. II ChIP-seq coverage tracks over chrXVI and bacterial chromosomes, and (ii) the average nucleosome, Scc1 or Pol. II ChIP-seq signal over 10kb random sequences with varying GC%.

**B**, Dinucleotide enrichment in genomic loci with 10% greatest nucleosome (left), Scc1 (middle) or Pol. II (right) ChIP-seq coverage (100 bp bins), extracted from experimental or predicted tracks over chromosome XVI, Mpneumo or Mmyco. The dinucleotide composition in these loci is compared to the chromosome-wide dinucleotide composition ( $\rho^*(XY)_{[\text{chromosome}]} / \rho^*(XY)_{[\text{chromosome}]}^*$ ).

**C**, Correlation scores between experimental and predicted nucleosome, Scc1 or Pol. II ChIP-seq data, using a linear model accounting for GC% only (green) or dinucleotide composition (kaki), or using CNNs (blue).

**D**, Motifs identified de novo as relevant for predicting nucleosome, Scc1 or Pol. II profiles.

Matches to similar motifs in yeast databases are shown on the left.

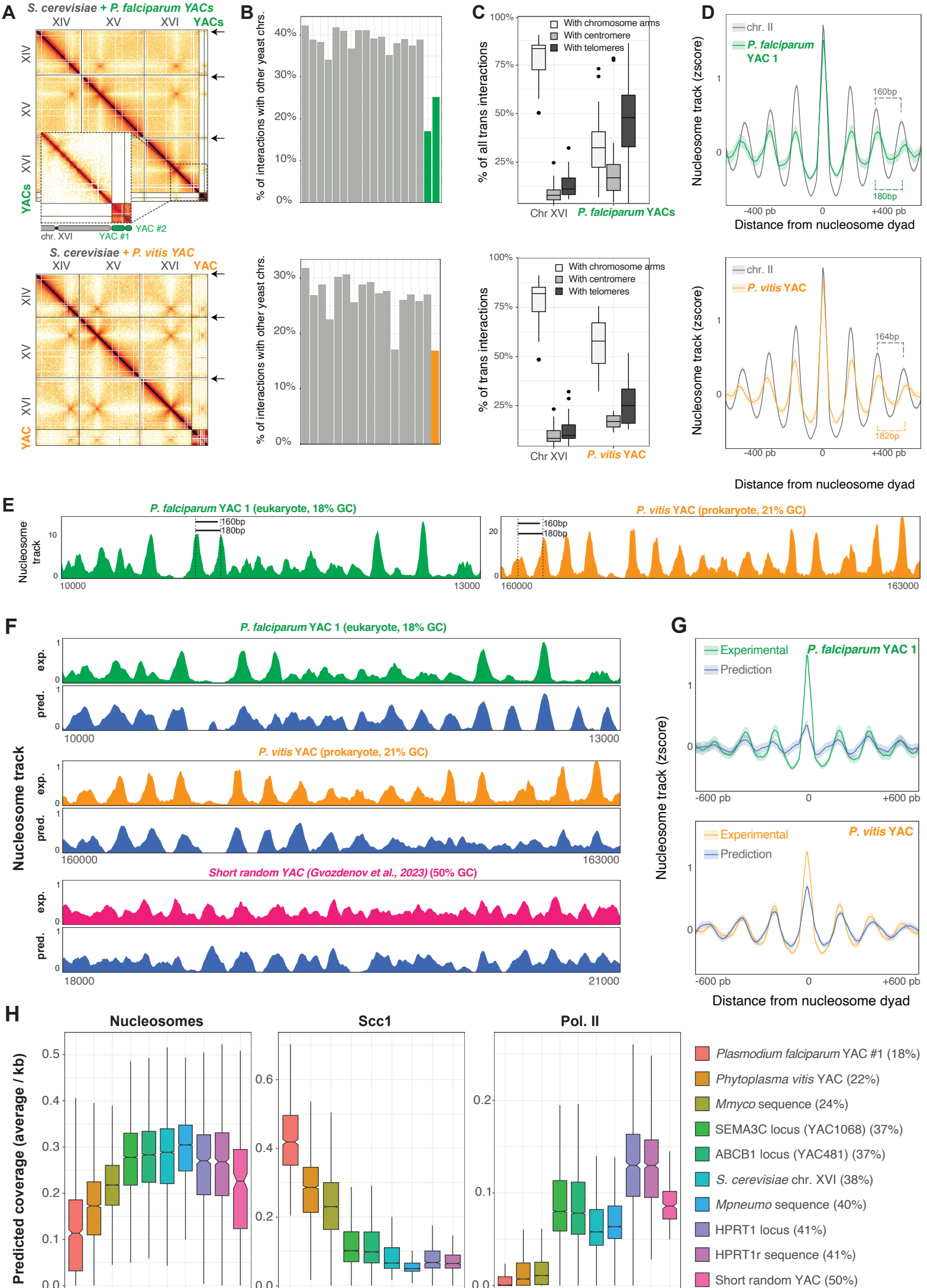


Fig. S10

**Fig. S10. U-type chromatin compartmentalization of AT-rich prokaryotic and eukaryotic YACs.**

**A**, Hi-C maps showing chromosomal interactions between *S. cerevisiae* chromosomes (XIV, XV, XVI) and artificial yeast chromosomes (YACs) from *P. falciparum* (top) and *P. vitis* (bottom). The inset for *P. falciparum* highlights the increased trans-chromosomal contacts between the two *P. falciparum* YACs in comparison with the decreased trans-chromosomal contacts between each of the YACs and the yeast chromosome XVI.

**B**, Percentage of interactions that each YAC has with yeast chromosomes.

**C**, Percentage of trans interactions between YACs and specific chromosomal regions (chromosome arms, centromere and telomeres), for *P. falciparum* (top) and *P. vitis* (bottom).

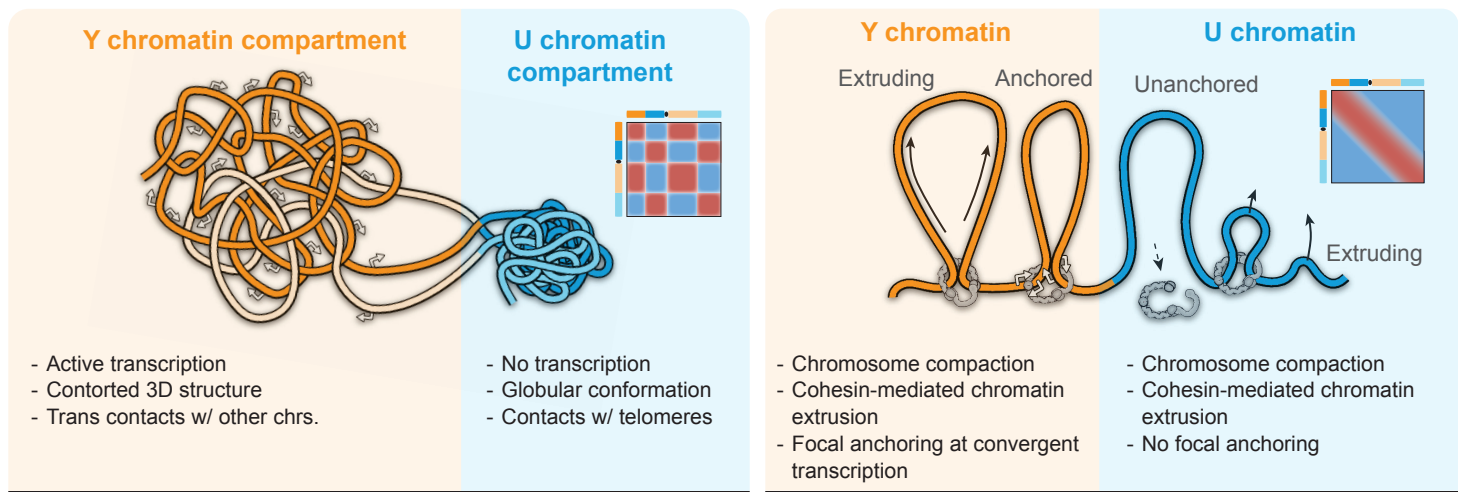
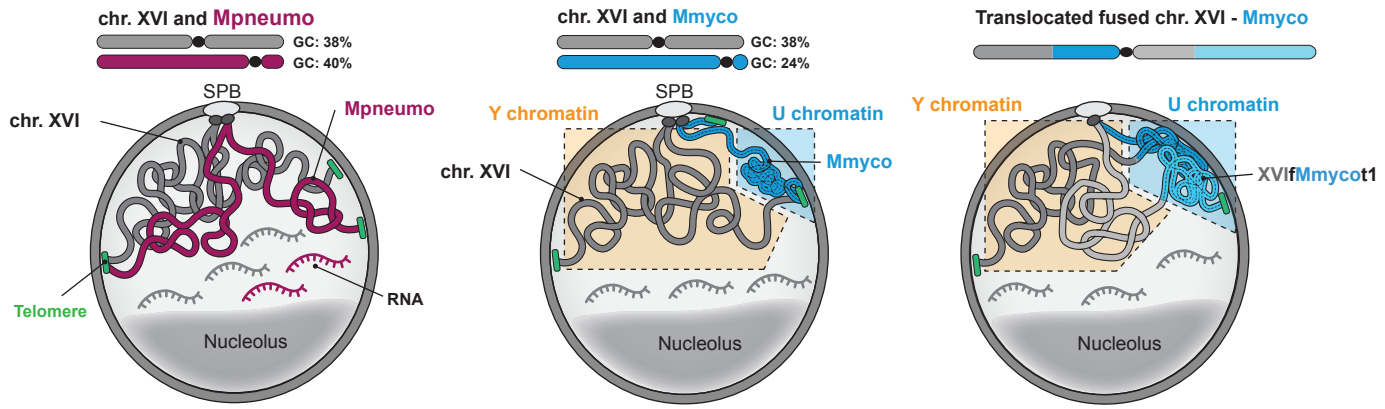
**D**, Average nucleosome signal centered at nucleosomes annotated over *P. falciparum* YAC (top, green) and *P. vitis* YAC (bottom, orange), compared to yeast nucleosomes (gray).

**E**, Nucleosome track over 3kb-wide segments of the *P. falciparum* YAC (left, green) or *P. vitis* YAC (right, orange).

**F**, Comparison of experimental (exp.) and predicted (pred.) nucleosome tracks for *P. falciparum* YAC (green), *P. vitis* YAC (orange), and a short random YAC (pink)(45).

**G**, Comparison of experimental (green or orange) and predicted nucleosome signals (dark blue), centered at nucleosomes annotated over *P. falciparum* YAC (top) and *P. vitis* YAC (bottom).

**H**, Predicted nucleosome, Scc1 and Pol. II coverages in chromosome sequences from different genomes. Coverage values are averaged using 1kb bins tiling each chromosome sequence.



**G1**

**G2/M**

**Fig. S11**

**Fig. S11. Behavior and activity of bacterial genomes integrated in the yeast genome.**

Illustration of the behaviors and activity of Mpneumo (left panel) and Mmyco (middle and right) chromosome sequences integrated in the yeast genome. Note that yeast and Mpneumo chromosomes intermingle in a single nuclear compartment, whereas the Mmyco chromosome (independently or in a chimeric state within chr. XVI) is condensed and segregated at the nuclear periphery, thereby defining the inactive U-type chromatin compartment.

**Table S1. Summary table of strains**

	Strains name	Description	Parental strain	Genetic background	MAT	Genotype	Reference
Mmmyco	RSG_Y711	Strain carrying the circular chromosome Mycoplasma mycoides subsp. mycoides strain PG1	W303	W303	a	ade2-1, leu2-3,112, his3-11,15, trp1-1, can1-100, RAD5 + M. mycoides circular genome with CEN6/ARS-HIS3	(16)
	RSG_Y712	Mmyco chromosome linearized	RSG_Y711	W303	a	ade2-1, leu2-3,112, his3-11,15, trp1-1, can1-100, RAD5 + M. mycoides linear genome with CEN6/ARS-HIS3	this study
	RSG_Y951	Mmyco chromosome linearized, SCC1-PK9	RSG_Y712	W303	a	ade2-1, leu2-3,112, his3-11,15, trp1-1, can1-100, RAD5 + M. mycoides linear genome with CEN6/ARS-HIS3, SCC1-pk9::KanMX	this study
	RSG_Y955	Linearized Mmyco, ΔWAPL	RSG_Y712	W303	a	ade2-1, leu2-3,112, his3-11,15, trp1-1, can1-100, RAD5 + M. mycoides linear genome with CEN6/ARS-HIS3, Rad61::KanMX	this study
	RSG_Y1033	XVIIfMmyco : "Fused" strain, Mmyco chromosome merged with the XVI	RSG_Y712	W303	a	ade2-1, leu2-3,112, his3-11,15, trp1-1, can1-100, RAD5, XVIIfMmyco(CEN6/ARS-HIS3)	this study
	RSG_Y1053	XVIIfMmyco : "Fused" strain with SCC1-PK9	RSG_Y1033	W303	a	ade2-1, leu2-3,112, his3-11,15, trp1-1, can1-100, RAD5 + XVIIfMmyco : "Fused" strain with SCC1-PK9	this study
	RSG_Y1136	XVIIfMmycot1 : "Translocation n°1" strain	RSG_Y1033	W303	a	ade2-1, leu2-3,112, his3-11,15, trp1-1, can1-100, SCC1-pk9::KanMX, RAD5, XVIIfMmyco(CEN6/ARS-HIS3)	this study
	RSG_Y1146	"Translocation n°1" strain with SCC1-PK9	RSG_Y1136	W303	a	ade2-1, leu2-3,112, his3-11,15, trp1-1, can1-100, RAD5, XVIIfMmycot1(CEN6/ARS-HIS3)	this study
	RSG_Y001375	"Translocation n°1" strain, Δhh01	RSG_Y1136	W303	a	ade2-1, leu2-3,112, his3-11,15, trp1-1, can1-100, RAD5, Δhh01, XVIIfMmycot1(CEN6/ARS-HIS3)	this study
	RSG_Y1137	XVIIfMmycot2 : "Translocation n°2" strain (50 kb block)	RSG_Y1136	W303	a	ade2-1, leu2-3,112, his3-11,15, trp1-1, can1-100, RAD5, XVIIfMmycot2(CEN6/ARS-HIS3)	this study
	RSG_Y1147	"Translocation n°2" strain (50 kb block) with SCC1-PK9	RSG_Y1137	W303	a	ade2-1, leu2-3,112, his3-11,15, trp1-1, can1-100, RAD5, SCC1-pk9::KanMX, XVIIfMmycot2(CEN6/ARS-HIS3)	this study
	RSG_Y001237	XVIIfMmycot2' : "Translocation n°2" strain (15 kb block)	RSG_Y1136	W303	a	ade2-1, leu2-3,112, his3-11,15, trp1-1, can1-100, RAD5, XVIIfMmycot2'(CEN6/ARS-HIS3)	this study
	RSG_Y001268	XVIIfMmycot2' : "Translocation n°2" strain (15 kb block) strain with SCC1-PK9	RSG_Y001237	W303	a	ade2-1, leu2-3,112, his3-11,15, trp1-1, can1-100, RAD5, SCC1-pk9::KanMX, XVIIfMmycot2'(CEN6/ARS-HIS3)	this study
	RSG_Y1274	XVIIfMmycot3 : "Triple Translocation n" strain	RSG_Y1136	W303	a	ade2-1, leu2-3,112, his3-11,15, trp1-1, can1-100, RAD5, XVIIfMmycot3(CEN6/ARS-HIS3)	this study
	yLD126-36c	Control split dot assay	NA	W303	a	Met3p-CDC20, tetR-GFP, ura3-1::URA3tetO	(95)
	FB176	fluorescent spot on linear Mmyco	RSG_Y712	W303	a	ade2-1, leu2-3,112::LEU2::tetR-GFP, his3-11,15, trp1-1, can1-100, ura3-1, Met3p-CDC20, M. mycoides linear genome with CEN6/ARS-HIS3 carrying 40000-42000::URA3::NATtetO	this study

	FB200	Strain with linear Mmyco, and fluorescent spot on endogenous yeast chromosome	RSG_Y712	W303	a	ade2-1, leu2-3,112::LEU2::tetR-GFP, his3-11,15, trp1-1, can1-100, ura3-1::URA3tetO, Met3p-CDC20, M. mycoides linear genome with CEN6/ARS-HIS3	this study
Mpneumo	RSG_Y681	Strain carrying the <i>Mycoplasma pneumoniae</i> strain M129	VL6-48N	VL6-48N	alpha	trp1-Δ1, ura3-Δ1, ade2-101, his3-Δ200, lys2, met14 cir° + Mp circular genome with CEN6/ARS-HIS3	(17)
	RSG_Y960	Pneumo chromosome linearized	RSG_Y681	VL6-48N	a	trp1-Δ1, ura3-Δ1, ade2-101, his3-Δ200, lys2, met14 cir° + Mp linear genome with CEN6/ARS-HIS3	this study
	RSG_Y1037	XVIIfMpneumo : "Fused "strain, Mpneumo chromosome merged with the XVI	RSG_Y960	VL6-48N	a	trp1-Δ1, ura3-Δ1, ade2-101, his3-Δ200, lys2, met14 cir° + XVIIfMpneumo(CEN6/ARS-HIS3)	this study
	RSG_Y001349	XVIIfMpneumo, RNH1::HTP	RSG_Y1037	VL6-48N	a	trp1-Δ1, ura3-Δ1, ade2-101, his3-Δ200, lys2, met14 cir°, RNH1::HTP + XVIIfMpneumo(CEN6/ARS-HIS3)	this study
	RSG_Y001273	XVIIfMpneumo ; Δupf1	RSG_Y1037	VL6-48N	a	trp1-Δ1, ura3-Δ1, ade2-101, his3-Δ200, lys2, met14 cir° Δupf1::KanMX + XVIIfMpneumo(CEN6/ARS-HIS3),	this study
	RSG_Y001308	XVIIfMpneumo ; Δrrp6	RSG_Y1037	VL6-48N	a	trp1-Δ1, ura3-Δ1, ade2-101, his3-Δ200, lys2, met14 cir°, Δrrp6 + XVIIfMpneumo(CEN6/ARS-HIS3),	this study
	RSG_Y001298	XVIIfMpneumo ; Δupf1 and Δrrp6	RSG_Y0012 73	VL6-48N	a	trp1-Δ1, ura3-Δ1, ade2-101, his3-Δ200, lys2, met14 cir°, Δupf1::KanMX, Δrrp6 + XVIIfMpneumo(CEN6/ARS-HIS3),	this study
	RSG_Y1080	Pneumo chromosome linearized with SCC1-PK9	RSG_Y960	VL6-48N	a	trp1-Δ1, ura3-Δ1, ade2-101, his3-Δ200, lys2, met14 cir° + Mp linear genome with CEN6/ARS-HIS3, SCC1-pk9::KanMX	this study
	RSG_Y954	Pneumo chromosome linearized with delta WAPL	RSG_Y960	VL6-48N	a	trp1-Δ1, ura3-Δ1, ade2-101, his3-Δ200, lys2, met14 cir° + Mp linear genome with CEN6/ARS-HIS3, Rad61::KanMX	this study
"Control" strains	RSG_Y784	W303 strain + pRS313	W303	W303	a	his3-11, 15 trp11 leu2-3,112 ura3-1 ade2-1 can1-100 [HIS3]	this study
	RSG_Y1158	VL6-48N strain + pRS413	VL6-48N	VL6-48N	a	trp1-Δ1 ura3-Δ1 ade2-101 his3-Δ200 lys2 met14 cir [HIS3]	this study
	RSG_Y973	Glabrata strain with SCC1-PK9	<i>C. glabrata</i>	<i>C. glabrata</i>	a	Scc1PK9::NatMX	(70)
	W303 strain + scc1-pk	W303 strain + scc1-pk	W303	W303	a	Scc1-pk9::KanMX	(70)
YACs	RSG_Y001392	W303a + FDp92 <i>Candidatus vitis</i> , YAC of ~300kb - 22%GC	W303	W303	a	leu2-3,112 trp1-1 can1-100 ura3-1 ade2-1 his3-11,15	this study
	RSG_Y001388	W303a + 2 YACs of <i>Plasmodium falciparum</i>	AB1380	AB1380	a	tiV ura3 trp1 ade2-1can1-100lys2-1his5	(96)

**Table S2. gRNA sequence (CRISPR targeting).**

gRNA sequences					
	Name	Transformation expected	Target	gRNA 5' 3'	Plasmid used
Mmyco strains	RSG_B700	Chromosome linearisation	DSB on the circular Mmyco (@ 739,680 bp)	TCTGCTAATCCTGTTACCAAGTGG	pML107
	RSG_B1158	Fusion between the end of the chromosome XVI to the chromosome Mmyco (generation of XVIIfMmyco strain)	DSB next to the centromere of chr XVI (@ 555,995 bp)	TTAGAATTACGACAACATAACGG	pAEF5
			DSB next to the right telomere of chr XVI (@ 936,139 bp)	TGGTGTATATAGTGGCACCGGG	
	RSG_B1150	DSB next to the right telomere of Mmyco (@ 1,219,826 bp)		GCGTGGACAAAGGTACAACGAGG	pGZ110
	RSG_B1200	Translocation 1 (generation of XVIIfMmycot1 strain)	DSB in the middle of the left arm of XVIIfMmyco (XVI DNA, @ 506,748 bp)	GAGAGCACAGGTGTACTGGAGGG	pAEF5
			DSB in the middle of the right arm of XVIIfMmyco (Mmyco DNA, @ 1,379,095 bp)	ACTTATTAGAAAATGAGCAGTGG	
Mpneumo strains	RSG_B1201	Translocation 2 50 kb (generation of XVIIfMmycot2 strain)	DSB ~ 50kb from translocation 1 breakpoint on left arm of XVIIfMmycot1 (in XVI sequence; @ 1,691,364 bp)	CTAACATGTCTCACTCCCGCGG	pAEF5
			DSB ~ 50kb from translocation 1 breakpoint on right arm of XVIIfMmycot1 (in Mmyco sequence, @ 737,819 bp)	CGTTCATGTTATGTGAAAAGAGG	
Mpneumo strains	Name	Transformation expected	Target	gRNA 5' 3'	Plasmid used
		Chromosome linearisation	DSB on the circular Mpneumo (@ xxx,xxx bp)	GTCAACGGTCAAAAAAACCGAGG	pAEF5

**Table S3. DNA donor sequences.**



**Table S4. Primer sequences.**

Checking primers					
	Transformation expected	Purpose	Primers sequence forward 5' 3'	Primers sequence reverse 5' 3'	Amplicons Length
Mmyco	Linearisation	Circular loss	TTCCACTGAGCGTCAGACC	TGCCGCTTACCGGATACC	-
		Check telomere addition R	CGTTGCGAGGTACTAAAGGC	TGCCGCTTACCGGATACC	242
		Check telomere addition L	TTCCACTGAGCGTCAGACC	agagcggtcagtagcaatcc	294
	XVIIfMyco	Check loss centromere XVI	GCCCTAGATCAAACGTGATCCAG	CCGGTAGAAGCCTTGTACC	555
		Check fusion	CCCGCATAAGTACGTGTAGCT	CAGTGAAGCACCAGTTCTG	688
	XVIIfMycot1	Check translocation R	CGATGCATACGTTCCATC	CTGGTAATCTTGAGATCC	729
		Check translocation L	GAGGGTATAACACTGCATCG	CCATATCCAGCCATATTGC	1127
	XVIIfMycot2	Check translocation R	CTTGTGTCCTGTGAAAG	CCAGAAAATGCTTGAGTAGC	760
		Check translocation L	GCAGTCGTTCTCAAACGG	GCATAGAAATTCACATAGGC	903
Mpneumo	Transformation expected	Purpose	Primers sequence forward 5' 3'	Primers sequence reverse 5' 3'	Amplicons Length
	Linearisation	Circular loss	GGTGGGTAAAGGTAAAGC	cgaatTAGCATGCTGTTGC	-
		Check telomere addition R	ggattgtactgaccgtct	GGTGGGTAAAGGTAAAGC	215
		Check telomere addition L	gcctttagtacctcgcaacg	cgaatTAGCATGCTGTTGC	300

**Table S5. Hi-C statistics.**

	<b>HiC library</b>	<b>background</b>	<b>strain</b>	<b>stage</b>	<b>Total sequenced fragments</b>	<b>Aligned fragments</b>	<b>Fragments retained in map</b>
CH196	Hi-C of Mmyco strain (G2/M)	W303_Mmmyco	RSG_Y712	G2/M	302589048	261015801	66875527
CH02	Hi-C of Mmyco strain (G1)	W303_Mmmyco	RSG_Y712	G1	109056382	81014812	20087984
CH198	Hi-C of Mmyco strain (Wpl1 deletion, G2/M)	W303_Mmmyco	RSG_Y955	G2/M	41113718	35092403	12373773
CH195	Hi-C of Mpneumo strain (G2/M)	S288C_Mpneumo	RSG_Y960	G2/M	76019938	65125087	19632515
CH210	Hi-C of Mpneumo strain (G1)	S288C_Mpneumo	RSG_Y960	G1	71379048	60466145	12456326
CH197	Hi-C of Mpneumo strain (Wpl1 deletion, G2/M)	S288C_Mpneumo	RSG_Y954	G2/M	39684936	35230228	11676521
LM34	Hi-C of XVIIfMmyco strain (G2/M)	XVIIfMmyco	RSG_Y103_3	G2/M	56889456	42820436	9754819
LM33	Hi-C of XVIIfMmyco strain (G1)	XVIIfMmyco	RSG_Y103_3	G1	43712974	32935796	6683250
LM58	Hi-C of XVIIfMmycot1 strain (G2/M)	XVIIfMmycot1	RSG_Y113_6	G2/M	53729240	42557126	13123109
LM63	Hi-C of XVIIfMmycot1 strain (G1)	XVIIfMmycot1	RSG_Y113_6	G1	43841832	36113087	9330391
LM59	Hi-C of XVIIfMmycot2 strain (G2/M)	XVIIfMmycot2	RSG_Y113_7	G2/M	49569888	40547069	13600786
LM62	Hi-C of XVIIfMmycot2 strain (G1)	XVIIfMmycot2	RSG_Y113_7	G1	50005472	41366045	12902417
LM119	Hi-C of XVIIfMmycot3 strain (G2/M)	XVIIfMmycot3	RSG_Y123_5	G2/M			
LM122	Hi-C of XVIIfMmycot3 strain (G1)	XVIIfMmycot3	RSG_Y123_5	G1			

## References and Notes

1. J. Romiguier, V. Ranwez, E. J. P. Douzery, N. Galtier, Contrasting GC-content dynamics across 33 mammalian genomes: Relationship with life-history traits and chromosome sizes. *Genome Res.* **20**, 1001–1009 (2010). [doi:10.1101/gr.104372.109](https://doi.org/10.1101/gr.104372.109) Medline
2. J. Tajbakhsh, H. Luz, H. Bornfleth, S. Lampel, C. Cremer, P. Lichter, Spatial distribution of GC- and AT-rich DNA sequences within human chromosome territories. *Exp. Cell Res.* **255**, 229–237 (2000). [doi:10.1006/excr.1999.4780](https://doi.org/10.1006/excr.1999.4780) Medline
3. A. Valouev, S. M. Johnson, S. D. Boyd, C. L. Smith, A. Z. Fire, A. Sidow, Determinants of nucleosome organization in primary human cells. *Nature* **474**, 516–520 (2011). [doi:10.1038/nature10002](https://doi.org/10.1038/nature10002) Medline
4. G. P. Holmquist, Evolution of chromosome bands: Molecular ecology of noncoding DNA. *J. Mol. Evol.* **28**, 469–486 (1989). [doi:10.1007/BF02602928](https://doi.org/10.1007/BF02602928) Medline
5. L. Mirny, J. Dekker, Mechanisms of Chromosome Folding and Nuclear Organization: Their Interplay and Open Questions. *Cold Spring Harb. Perspect. Biol.* **14**, a040147 (2022). [doi:10.1101/cshperspect.a040147](https://doi.org/10.1101/cshperspect.a040147) Medline
6. I. F. Davidson, J.-M. Peters, Genome folding through loop extrusion by SMC complexes. *Nat. Rev. Mol. Cell Biol.* **22**, 445–464 (2021). [doi:10.1038/s41580-021-00349-7](https://doi.org/10.1038/s41580-021-00349-7) Medline
7. A. S. Belmont, Nuclear Compartments: An Incomplete Primer to Nuclear Compartments, Bodies, and Genome Organization Relative to Nuclear Architecture. *Cold Spring Harb. Perspect. Biol.* **14**, a041268 (2022). [doi:10.1101/cshperspect.a041268](https://doi.org/10.1101/cshperspect.a041268) Medline
8. A. Crisp, C. Boschetti, M. Perry, A. Tunnacliffe, G. Micklem, Expression of multiple horizontally acquired genes is a hallmark of both vertebrate and invertebrate genomes. *Genome Biol.* **16**, 50 (2015). [doi:10.1186/s13059-015-0607-3](https://doi.org/10.1186/s13059-015-0607-3) Medline
9. N. B. Edelman, J. Mallet, Prevalence and Adaptive Impact of Introgression. *Annu. Rev. Genet.* **55**, 265–283 (2021). [doi:10.1146/annurev-genet-021821-020805](https://doi.org/10.1146/annurev-genet-021821-020805) Medline
10. J. Van Etten, D. Bhattacharya, Horizontal Gene Transfer in Eukaryotes: Not if, but How Much? *Trends Genet.* **36**, 915–925 (2020). [doi:10.1016/j.tig.2020.08.006](https://doi.org/10.1016/j.tig.2020.08.006) Medline
11. J. Peter, M. De Chiara, A. Friedrich, J.-X. Yue, D. Pflieger, A. Bergström, A. Sigwalt, B. Barre, K. Freel, A. Llored, C. Cruaud, K. Labadie, J.-M. Aury, B. Istace, K. Lebrigand, P. Barbry, S. Engelen, A. Lemainque, P. Wincker, G. Liti, J. Schacherer, Genome evolution across 1,011 *Saccharomyces cerevisiae* isolates. *Nature* **556**, 339–344 (2018). [doi:10.1038/s41586-018-0030-5](https://doi.org/10.1038/s41586-018-0030-5) Medline
12. V. Baby, F. Labroussaa, J. Brodeur, D. Matteau, G. Gourgues, C. Lartigue, S. Rodrigue, Cloning and Transplantation of the *Mesoplasma florum* Genome. *ACS Synth. Biol.* **7**, 209–217 (2018). [doi:10.1021/acssynbio.7b00279](https://doi.org/10.1021/acssynbio.7b00279) Medline
13. A. L. V. Coradini, C. B. Hull, I. M. Ehrenreich, Building genomes to understand biology. *Nat. Commun.* **11**, 6177 (2020). [doi:10.1038/s41467-020-19753-2](https://doi.org/10.1038/s41467-020-19753-2) Medline
14. A. Currin, S. Parker, C. J. Robinson, E. Takano, N. S. Scrutton, R. Breitling, The evolving art of creating genetic diversity: From directed evolution to synthetic biology. *Biotechnol. Adv.* **50**, 107762 (2021). [doi:10.1016/j.biotechadv.2021.107762](https://doi.org/10.1016/j.biotechadv.2021.107762) Medline

15. C. Payen, G. Fischer, C. Marck, C. Proux, D. J. Sherman, J.-Y. Coppée, M. Johnston, B. Dujon, C. Neuvéglise, Unusual composition of a yeast chromosome arm is associated with its delayed replication. *Genome Res.* **19**, 1710–1721 (2009).  
[doi:10.1101/gr.090605.108](https://doi.org/10.1101/gr.090605.108) [Medline](#)
16. F. Labroussaa, A. Lebaudy, V. Baby, G. Gourgues, D. Matteau, S. Vashee, P. Sirand-Pugnet, S. Rodrigue, C. Lartigue, Impact of donor-recipient phylogenetic distance on bacterial genome transplantation. *Nucleic Acids Res.* **44**, 8501–8511 (2016).  
[doi:10.1093/nar/gkw688](https://doi.org/10.1093/nar/gkw688) [Medline](#)
17. E. Ruiz, V. Talenton, M.-P. Dubrana, G. Guesdon, M. Lluch-Senar, F. Salin, P. Sirand-Pugnet, Y. Arfi, C. Lartigue, CReasPy-Cloning: A Method for Simultaneous Cloning and Engineering of Megabase-Sized Genomes in Yeast Using the CRISPR-Cas9 System. *ACS Synth. Biol.* **8**, 2547–2557 (2019). [doi:10.1021/acssynbio.9b00224](https://doi.org/10.1021/acssynbio.9b00224) [Medline](#)
18. C. Lartigue, S. Vashee, M. A. Algire, R.-Y. Chuang, G. A. Benders, L. Ma, V. N. Noskov, E. A. Denisova, D. G. Gibson, N. Assad-Garcia, N. Alperovich, D. W. Thomas, C. Merryman, C. A. Hutchison 3rd, H. O. Smith, J. C. Venter, J. I. Glass, Creating bacterial strains from genomes that have been cloned and engineered in yeast. *Science* **325**, 1693–1696 (2009). [doi:10.1126/science.1173759](https://doi.org/10.1126/science.1173759) [Medline](#)
19. S. Karlin, J. Mrázek, Compositional differences within and between eukaryotic genomes. *Proc. Natl. Acad. Sci. U.S.A.* **94**, 10227–10232 (1997). [doi:10.1073/pnas.94.19.10227](https://doi.org/10.1073/pnas.94.19.10227) [Medline](#)
20. K. Nasmyth, Disseminating the genome: Joining, resolving, and separating sister chromatids during mitosis and meiosis. *Annu. Rev. Genet.* **35**, 673–745 (2001).  
[doi:10.1146/annurev.genet.35.102401.091334](https://doi.org/10.1146/annurev.genet.35.102401.091334) [Medline](#)
21. K. Brogaard, L. Xi, J.-P. Wang, J. Widom, A map of nucleosome positions in yeast at base-pair resolution. *Nature* **486**, 496–501 (2012). [doi:10.1038/nature11142](https://doi.org/10.1038/nature11142) [Medline](#)
22. M. T. Ocampo-Hafalla, Y. Katou, K. Shirahige, F. Uhlmann, Displacement and re-accumulation of centromeric cohesin during transient pre-anaphase centromere splitting. *Chromosoma* **116**, 531–544 (2007). [doi:10.1007/s00412-007-0118-4](https://doi.org/10.1007/s00412-007-0118-4) [Medline](#)
23. K.-L. Chan, M. B. Roig, B. Hu, F. Beckouët, J. Metson, K. Nasmyth, Cohesin’s DNA exit gate is distinct from its entrance gate and is regulated by acetylation. *Cell* **150**, 961–974 (2012). [doi:10.1016/j.cell.2012.07.028](https://doi.org/10.1016/j.cell.2012.07.028) [Medline](#)
24. D. Challal, M. Barucco, S. Kubik, F. Feuerbach, T. Candelli, H. Geoffroy, C. Benaksas, D. Shore, D. Libri, General Regulatory Factors Control the Fidelity of Transcription by Restricting Non-coding and Ectopic Initiation. *Mol. Cell* **72**, 955–969.e7 (2018).  
[doi:10.1016/j.molcel.2018.11.037](https://doi.org/10.1016/j.molcel.2018.11.037) [Medline](#)
25. L. Lazar-Stefanita, V. F. Scolari, G. Mercy, H. Muller, T. M. Guérin, A. Thierry, J. Mozziconacci, R. Koszul, Cohesins and condensins orchestrate the 4D dynamics of yeast chromosomes during the cell cycle. *EMBO J.* **36**, 2684–2697 (2017).  
[doi:10.15252/embj.201797342](https://doi.org/10.15252/embj.201797342) [Medline](#)
26. Z. Duan, M. Andronescu, K. Schutz, S. McIlwain, Y. J. Kim, C. Lee, J. Shendure, S. Fields, C. A. Blau, W. S. Noble, A three-dimensional model of the yeast genome. *Nature* **465**, 363–367 (2010). [doi:10.1038/nature08973](https://doi.org/10.1038/nature08973) [Medline](#)

27. H. Wong, H. Marie-Nelly, S. Herbert, P. Carrivain, H. Blanc, R. Koszul, E. Fabre, C. Zimmer, A predictive computational model of the dynamic 3D interphase yeast nucleus. *Curr. Biol.* **22**, 1881–1890 (2012). [doi:10.1016/j.cub.2012.07.069](https://doi.org/10.1016/j.cub.2012.07.069) Medline
28. A. Y. Grosberg, S. K. Nechaev, E. I. Shakhnovich, The role of topological constraints in the kinetics of collapse of macromolecules. *J. Phys. (Paris)* **49**, 2095–2100 (1988). [doi:10.1051/jphys:0198800490120209500](https://doi.org/10.1051/jphys:0198800490120209500)
29. L. A. Mirny, The fractal globule as a model of chromatin architecture in the cell. *Chromosome Res.* **19**, 37–51 (2011). [doi:10.1007/s10577-010-9177-0](https://doi.org/10.1007/s10577-010-9177-0) Medline
30. A. Taddei, S. M. Gasser, Structure and function in the budding yeast nucleus. *Genetics* **192**, 107–129 (2012). [doi:10.1534/genetics.112.140608](https://doi.org/10.1534/genetics.112.140608) Medline
31. L. Dauban, R. Montagne, A. Thierry, L. Lazar-Stefanita, N. Bastié, O. Gadal, A. Cournac, R. Koszul, F. Beckouët, Regulation of Cohesin-Mediated Chromosome Folding by Eco1 and Other Partners. *Mol. Cell* **77**, 1279–1293.e4 (2020). [doi:10.1016/j.molcel.2020.01.019](https://doi.org/10.1016/j.molcel.2020.01.019) Medline
32. L. Costantino, T. S. Hsieh, R. Lamothe, X. Darzacq, D. Koshland, Cohesin residency determines chromatin loop patterns. *eLife* **9**, 59889 (2020). [doi:10.7554/eLife.59889](https://doi.org/10.7554/eLife.59889) Medline
33. S. A. Schalbetter, A. Goloborodko, G. Fudenberg, J.-M. Belton, C. Miles, M. Yu, J. Dekker, L. Mirny, J. Baxter, SMC complexes differentially compact mitotic chromosomes according to genomic context. *Nat. Cell Biol.* **19**, 1071–1080 (2017). [doi:10.1038/ncb3594](https://doi.org/10.1038/ncb3594) Medline
34. S. S. P. Rao, M. H. Huntley, N. C. Durand, E. K. Stamenova, I. D. Bochkov, J. T. Robinson, A. L. Sanborn, I. Machol, A. D. Omer, E. S. Lander, E. L. Aiden, A 3D map of the human genome at kilobase resolution reveals principles of chromatin looping. *Cell* **159**, 1665–1680 (2014). [doi:10.1016/j.cell.2014.11.021](https://doi.org/10.1016/j.cell.2014.11.021) Medline
35. A. Goloborodko, M. V. Imakaev, J. F. Marko, L. Mirny, Compaction and segregation of sister chromatids via active loop extrusion. *eLife* **5**, e14864 (2016). [doi:10.7554/eLife.14864](https://doi.org/10.7554/eLife.14864) Medline
36. J. H. I. Haarhuis, R. H. van der Weide, V. A. Blomen, J. O. Yáñez-Cuna, M. Amendola, M. S. van Ruiten, P. H. L. Krijger, H. Teunissen, R. H. Medema, B. van Steensel, T. R. Brummelkamp, E. de Wit, B. D. Rowland, The Cohesin Release Factor WAPL Restricts Chromatin Loop Extension. *Cell* **169**, 693–707.e14 (2017). [doi:10.1016/j.cell.2017.04.013](https://doi.org/10.1016/j.cell.2017.04.013) Medline
37. E. Lieberman-Aiden, N. L. van Berkum, L. Williams, M. Imakaev, T. Ragoczy, A. Telling, I. Amit, B. R. Lajoie, P. J. Sabo, M. O. Dorschner, R. Sandstrom, B. Bernstein, M. A. Bender, M. Groudine, A. Gnirke, J. Stamatoyannopoulos, L. A. Mirny, E. S. Lander, J. Dekker, Comprehensive mapping of long-range interactions reveals folding principles of the human genome. *Science* **326**, 289–293 (2009). [doi:10.1126/science.1181369](https://doi.org/10.1126/science.1181369) Medline
38. N. Naumova, M. Imakaev, G. Fudenberg, Y. Zhan, B. R. Lajoie, L. A. Mirny, J. Dekker, Organization of the Mitotic Chromosome. *Science* **342**, 948–953 (2013). [doi:10.1126/science.1236083](https://doi.org/10.1126/science.1236083) Medline

39. J. H. Gibcus, K. Samejima, A. Goloborodko, I. Samejima, N. Naumova, J. Nuebler, M. T. Kanemaki, L. Xie, J. R. Paulson, W. C. Earnshaw, L. A. Mirny, J. Dekker, A pathway for mitotic chromosome formation. *Science* **359**, eaao6135 (2018). [doi:10.1126/science.aao6135](https://doi.org/10.1126/science.aao6135) [Medline](#)
40. G. Spracklin, N. Abdennur, M. Imakaev, N. Chowdhury, S. Pradhan, L. A. Mirny, J. Dekker, Diverse silent chromatin states modulate genome compartmentalization and loop extrusion barriers. *Nat. Struct. Mol. Biol.* **30**, 38–51 (2023). [doi:10.1038/s41594-022-00892-7](https://doi.org/10.1038/s41594-022-00892-7) [Medline](#)
41. E. P. Nora, Targeted Degradation of CTCF Decouples Local Insulation of Chromosome Domains from Genomic Compartmentalization. *Cell* **169**, 930–944.e22 (2017). [doi:10.1016/j.cell.2017.05.004](https://doi.org/10.1016/j.cell.2017.05.004) [Medline](#)
42. M. Kabi, G. J. Filion, Heterochromatin: Did H3K9 methylation evolve to tame transposons? *Genome Biol.* **22**, 325 (2021). [doi:10.1186/s13059-021-02550-5](https://doi.org/10.1186/s13059-021-02550-5) [Medline](#)
43. M. R. Gartenberg, J. S. Smith, The Nuts and Bolts of Transcriptionally Silent Chromatin in *Saccharomyces cerevisiae*. *Genetics* **203**, 1563–1599 (2016). [doi:10.1534/genetics.112.145243](https://doi.org/10.1534/genetics.112.145243) [Medline](#)
44. L. L. Breedon, T. Tsukiyama, Quiescence in *Saccharomyces cerevisiae*. *Annu. Rev. Genet.* **56**, 253–278 (2022). [doi:10.1146/annurev-genet-080320-023632](https://doi.org/10.1146/annurev-genet-080320-023632) [Medline](#)
45. M. Guidi, M. Ruault, M. Marbouty, I. Loïodice, A. Cournac, C. Billaudeau, A. Hocher, J. Mozziconacci, R. Koszul, A. Taddei, Spatial reorganization of telomeres in long-lived quiescent cells. *Genome Biol.* **16**, 206 (2015). [doi:10.1186/s13059-015-0766-2](https://doi.org/10.1186/s13059-015-0766-2) [Medline](#)
46. K. Struhl, E. Segal, Determinants of nucleosome positioning. *Nat. Struct. Mol. Biol.* **20**, 267–273 (2013). [doi:10.1038/nsmb.2506](https://doi.org/10.1038/nsmb.2506) [Medline](#)
47. E. Routhier, E. Pierre, G. Khodabandelou, J. Mozziconacci, Genome-wide prediction of DNA mutation effect on nucleosome positions for yeast synthetic genomics. *Genome Res.* **31**, 317–326 (2021). [doi:10.1101/gr.264416.120](https://doi.org/10.1101/gr.264416.120) [Medline](#)
48. R. V. Chereji, D. J. Clark, Major Determinants of Nucleosome Positioning. *Biophys. J.* **114**, 2279–2289 (2018). [doi:10.1016/j.bpj.2018.03.015](https://doi.org/10.1016/j.bpj.2018.03.015) [Medline](#)
49. Z. Gvozdenov, Z. Barcutean, K. Struhl, Functional analysis of a random-sequence chromosome reveals a high level and the molecular nature of transcriptional noise in yeast cells. *Mol. Cell* **83**, 1786–1797.e5 (2023). [doi:10.1016/j.molcel.2023.04.010](https://doi.org/10.1016/j.molcel.2023.04.010) [Medline](#)
50. B. R. Camellato, R. Brosh, H. J. Ashe, M. T. Maurano, J. D. Boeke, Synthetic reversed sequences reveal default genomic states. *Nature* **628**, 373–380 (2024). [doi:10.1038/s41586-024-07128-2](https://doi.org/10.1038/s41586-024-07128-2) [Medline](#)
51. I. Luthra, C. Jensen, X. E. Chen, A. L. Salaudeen, A. M. Rafi, C. G. de Boer, Regulatory activity is the default DNA state in eukaryotes. *Nat. Struct. Mol. Biol.* **31**, 559–567 (2024). [doi:10.1038/s41594-024-01235-4](https://doi.org/10.1038/s41594-024-01235-4) [Medline](#)
52. P. A. Ginno, P. L. Lott, H. C. Christensen, I. Korf, F. Chédin, R-loop formation is a distinctive characteristic of unmethylated human CpG island promoters. *Mol. Cell* **45**, 814–825 (2012). [doi:10.1016/j.molcel.2012.01.017](https://doi.org/10.1016/j.molcel.2012.01.017) [Medline](#)

53. J. R. Lobry, Asymmetric substitution patterns in the two DNA strands of bacteria. *Mol. Biol. Evol.* **13**, 660–665 (1996). [doi:10.1093/oxfordjournals.molbev.a025626](https://doi.org/10.1093/oxfordjournals.molbev.a025626) Medline
54. N. Bastié, C. Chapard, A. Cournac, S. Nejmi, H. Mboumba, O. Gadal, A. Thierry, F. Beckouët, R. Koszul, Sister chromatid cohesion halts DNA loop expansion. *Mol. Cell* **84**, 1139–1148.e5 (2024). [doi:10.1016/j.molcel.2024.02.004](https://doi.org/10.1016/j.molcel.2024.02.004) Medline
55. E. J. Banigan, W. Tang, A. A. van den Berg, R. R. Stocsits, G. Wutz, H. B. Brandão, G. A. Busslinger, J.-M. Peters, L. A. Mirny, Transcription shapes 3D chromatin organization by interacting with loop extrusion. *Proc. Natl. Acad. Sci. U.S.A.* **120**, e2210480120 (2023). [doi:10.1073/pnas.2210480120](https://doi.org/10.1073/pnas.2210480120) Medline
56. B. J. H. Dequeker, M. J. Scherr, H. B. Brandão, J. Gassler, S. Powell, I. Gaspar, I. M. Flyamer, A. Lalic, W. Tang, R. Stocsits, I. F. Davidson, J.-M. Peters, K. E. Duderstadt, L. A. Mirny, K. Tachibana, MCM complexes are barriers that restrict cohesin-mediated loop extrusion. *Nature* **606**, 197–203 (2022). [doi:10.1038/s41586-022-04730-0](https://doi.org/10.1038/s41586-022-04730-0) Medline
57. M. Falk, Y. Feodorova, N. Naumova, M. Imakaev, B. R. Lajoie, H. Leonhardt, B. Joffe, J. Dekker, G. Fudenberg, I. Solovei, L. A. Mirny, Heterochromatin drives compartmentalization of inverted and conventional nuclei. *Nature* **570**, 395–399 (2019). [doi:10.1038/s41586-019-1275-3](https://doi.org/10.1038/s41586-019-1275-3) Medline
58. F. Zenk, Y. Zhan, P. Kos, E. Löser, N. Atinbayeva, M. Schächtle, G. Tiana, L. Giorgetti, N. Iovino, HP1 drives de novo 3D genome reorganization in early *Drosophila* embryos. *Nature* **593**, 289–293 (2021). [doi:10.1038/s41586-021-03460-z](https://doi.org/10.1038/s41586-021-03460-z) Medline
59. H. Zhao, Y. Lin, E. Lin, F. Liu, L. Shu, D. Jing, B. Wang, M. Wang, F. Shan, L. Zhang, J. C. Lam, S. C. Midla, B. M. Giardine, C. A. Keller, R. C. Hardison, G. A. Blobel, H. Zhang, Genome folding principles uncovered in condensin-depleted mitotic chromosomes. *Nat. Genet.* **56**, 1213–1224 (2024). [doi:10.1038/s41588-024-01759-x](https://doi.org/10.1038/s41588-024-01759-x) Medline
60. T. S. Hsieh, C. Cattoglio, E. Slobodyanyuk, A. S. Hansen, O. J. Rando, R. Tjian, X. Darzacq, Resolving the 3D Landscape of Transcription-Linked Mammalian Chromatin Folding. *Mol. Cell* **78**, 539–553.e8 (2020). [doi:10.1016/j.molcel.2020.03.002](https://doi.org/10.1016/j.molcel.2020.03.002) Medline
61. C. Allen, S. Büttner, A. D. Aragon, J. A. Thomas, O. Meirelles, J. E. Jaetao, D. Benn, S. W. Ruby, M. Veenhuis, F. Madeo, M. Werner-Washburne, Isolation of quiescent and nonquiescent cells from yeast stationary-phase cultures. *J. Cell Biol.* **174**, 89–100 (2006). [doi:10.1083/jcb.200604072](https://doi.org/10.1083/jcb.200604072) Medline
62. M. F. Laughery, T. Hunter, A. Brown, J. Hoopes, T. Ostbye, T. Shumaker, J. J. Wyrick, New vectors for simple and streamlined CRISPR-Cas9 genome editing in *Saccharomyces cerevisiae*. *Yeast* **32**, 711–720 (2015). [doi:10.1002/yea.3098](https://doi.org/10.1002/yea.3098) Medline
63. N. Agier, A. Fleiss, S. Delmas, G. Fischer, A Versatile Protocol to Generate Translocations in Yeast Genomes Using CRISPR/Cas9. *Methods Mol. Biol.* **2196**, 181–198 (2021). [doi:10.1007/978-1-0716-0868-5\\_14](https://doi.org/10.1007/978-1-0716-0868-5_14) Medline
64. J. Luo, X. Sun, B. P. Cormack, J. D. Boeke, Karyotype engineering by chromosome fusion leads to reproductive isolation in yeast. *Nature* **560**, 392–396 (2018). [doi:10.1038/s41586-018-0374-x](https://doi.org/10.1038/s41586-018-0374-x) Medline

65. K. Labun, T. G. Montague, M. Krause, Y. N. Torres Cleuren, H. Tjeldnes, E. Valen, CHOPCHOP v3: Expanding the CRISPR web toolbox beyond genome editing. *Nucleic Acids Res.* **47** (W1), W171–W174 (2019). [doi:10.1093/nar/gkz365](https://doi.org/10.1093/nar/gkz365) [Medline](#)
66. J.-P. Concordet, M. Haeussler, CRISPOR: Intuitive guide selection for CRISPR/Cas9 genome editing experiments and screens. *Nucleic Acids Res.* **46**, W242–W245 (2018). [doi:10.1093/nar/gky354](https://doi.org/10.1093/nar/gky354) [Medline](#)
67. T. W. Christianson, R. S. Sikorski, M. Dante, J. H. Shero, P. Hieter, Multifunctional yeast high-copy-number shuttle vectors. *Gene* **110**, 119–122 (1992). [doi:10.1016/0378-1119\(92\)90454-W](https://doi.org/10.1016/0378-1119(92)90454-W) [Medline](#)
68. R. Koszul, S. Caburet, B. Dujon, G. Fischer, Eucaryotic genome evolution through the spontaneous duplication of large chromosomal segments. *EMBO J.* **23**, 234–243 (2004). [doi:10.1038/sj.emboj.7600024](https://doi.org/10.1038/sj.emboj.7600024) [Medline](#)
69. D. Viterbo, A. Marchal, V. Mosbach, L. Poggi, W. Vaysse-Zinkhöfer, G.-F. Richard, A fast, sensitive and cost-effective method for nucleic acid detection using non-radioactive probes. *Biol. Methods Protoc.* **3**, bpy006 (2018). [doi:10.1093/biometRICS/bpy006](https://doi.org/10.1093/biometRICS/bpy006) [Medline](#)
70. B. Hu, N. Petela, A. Kurze, K.-L. Chan, C. Chapard, K. Nasmyth, Biological chromodynamics: A general method for measuring protein occupancy across the genome by calibrating ChIP-seq. *Nucleic Acids Res.* **43**, e132 (2015). [doi:10.1093/nar/gkv670](https://doi.org/10.1093/nar/gkv670) [Medline](#)
71. S. Granneman, G. Kudla, E. Petfalski, D. Tollervey, Identification of protein binding sites on U3 snoRNA and pre-rRNA by UV cross-linking and high-throughput analysis of cDNAs. *Proc. Natl. Acad. Sci. U.S.A.* **106**, 9613–9618 (2009). [doi:10.1073/pnas.0901997106](https://doi.org/10.1073/pnas.0901997106) [Medline](#)
72. B. Langmead, S. L. Salzberg, Fast gapped-read alignment with Bowtie 2. *Nat. Methods* **9**, 357–359 (2012). [doi:10.1038/nmeth.1923](https://doi.org/10.1038/nmeth.1923) [Medline](#)
73. A. Courzac, H. Marie-Nelly, M. Marbouty, R. Koszul, J. Mozziconacci, Normalization of a chromosomal contact map. *BMC Genomics* **13**, 436 (2012). [doi:10.1186/1471-2164-13-436](https://doi.org/10.1186/1471-2164-13-436) [Medline](#)
74. N. Abdennur, L. A. Mirny, Cooler: Scalable storage for Hi-C data and other genomically labeled arrays. *Bioinformatics* **36**, 311–316 (2020). [doi:10.1093/bioinformatics/btz540](https://doi.org/10.1093/bioinformatics/btz540) [Medline](#)
75. F. Ramírez, D. P. Ryan, B. Grüning, V. Bhardwaj, F. Kilpert, A. S. Richter, S. Heyne, F. Dündar, T. Manke, deepTools2: A next generation web server for deep-sequencing data analysis. *Nucleic Acids Res.* **44**, W160–5 (2016). [doi:10.1093/nar/gkw257](https://doi.org/10.1093/nar/gkw257) [Medline](#)
76. P. Danecek, J. K. Bonfield, J. Liddle, J. Marshall, V. Ohan, M. O. Pollard, A. Whitwham, T. Keane, S. A. McCarthy, R. M. Davies, H. Li, Twelve years of SAMtools and BCFtools. *Gigascience* **10**, giab008 (2021). [doi:10.1093/gigascience/giab008](https://doi.org/10.1093/gigascience/giab008) [Medline](#)
77. J. Serizay, R. Koszul, Epigenomics coverage data extraction and aggregation in R with tidyCoverage. *Bioinformatics* **40**, btae487 (2024). [doi:10.1093/bioinformatics/btae487](https://doi.org/10.1093/bioinformatics/btae487) [Medline](#)

78. J. Serizay, C. Matthey-Doret, A. Bignaud, L. Baudry, R. Koszul, Orchestrating chromosome conformation capture analysis with Bioconductor. *Nat. Commun.* **15**, 1072 (2024). [doi:10.1038/s41467-024-44761-x](https://doi.org/10.1038/s41467-024-44761-x) [Medline](#)
79. Y. Liao, G. K. Smyth, W. Shi, featureCounts: An efficient general purpose program for assigning sequence reads to genomic features. *Bioinformatics* **30**, 923–930 (2014). [doi:10.1093/bioinformatics/btt656](https://doi.org/10.1093/bioinformatics/btt656) [Medline](#)
80. M. I. Love, W. Huber, S. Anders, Moderated estimation of fold change and dispersion for RNA-seq data with DESeq2. *Genome Biol.* **15**, 550 (2014). [doi:10.1186/s13059-014-0550-8](https://doi.org/10.1186/s13059-014-0550-8) [Medline](#)
81. J. Serizay, J. Ahringer, periodicDNA: An R/Bioconductor package to investigate k-mer periodicity in DNA. *F1000 Res.* **10**, 141 (2021). [doi:10.12688/f1000research.51143.1](https://doi.org/10.12688/f1000research.51143.1) [Medline](#)
82. M. Jiang, J. Anderson, J. Gillespie, M. Mayne, uShuffle: A useful tool for shuffling biological sequences while preserving the k-let counts. *BMC Bioinformatics* **9**, 192 (2008). [doi:10.1186/1471-2105-9-192](https://doi.org/10.1186/1471-2105-9-192) [Medline](#)
83. C. Matthey-Doret, L. Baudry, A. Breuer, R. Montagne, N. Guiglielmoni, V. Scolari, E. Jean, A. Campeas, P. H. Chanut, E. Oriol, A. Méot, L. Politis, A. Vigouroux, P. Moreau, R. Koszul, A. Couranc, Computer vision for pattern detection in chromosome contact maps. *Nat. Commun.* **11**, 5795 (2020). [doi:10.1038/s41467-020-19562-7](https://doi.org/10.1038/s41467-020-19562-7) [Medline](#)
84. Keras 3: A new multi-backend Keras, Keras (2023); <https://github.com/keras-team/keras>.
85. M. Abadi, P. Barham, J. Chen, Z. Chen, A. Davis, J. Dean, M. Devin, S. Ghemawat, G. Irving, M. Isard, M. Kudlur, J. Levenberg, R. Monga, S. Moore, D. G. Murray, B. Steiner, P. Tucker, V. Vasudevan, P. Warden, M. Wicke, Y. Yu, X. Zheng, “TensorFlow: a system for large-scale machine learning” in *Proceedings of the 12th USENIX Conference on Operating Systems Design and Implementation* (USENIX Association, 2016), pp. 265–283.
86. E. Routhier, A. B. Kamruddin, J. Mozziconacci, keras\_dna: a wrapper for fast implementation of deep learning models in genomics. *Bioinformatics* **37**, 1593–1594 (2021). [doi:10.1093/bioinformatics/btaa929](https://doi.org/10.1093/bioinformatics/btaa929) [Medline](#)
87. D. R. Kelley, Y. A. Reshef, M. Bileschi, D. Belanger, C. Y. McLean, J. Snoek, Sequential regulatory activity prediction across chromosomes with convolutional neural networks. *Genome Res.* **28**, 739–750 (2018). [doi:10.1101/gr.227819.117](https://doi.org/10.1101/gr.227819.117) [Medline](#)
88. A. Majdandzic, C. Rajesh, P. K. Koo, Correcting gradient-based interpretations of deep neural networks for genomics. *Genome Biol.* **24**, 109 (2023). [doi:10.1186/s13059-023-02956-3](https://doi.org/10.1186/s13059-023-02956-3) [Medline](#)
89. T. L. Bailey, J. Johnson, C. E. Grant, W. S. Noble, The MEME Suite. *Nucleic Acids Res.* **43**, W39–W49 (2015). [doi:10.1093/nar/gkv416](https://doi.org/10.1093/nar/gkv416) [Medline](#)
90. M. Gotta, T. Laroche, S. M. Gasser, Analysis of nuclear organization in *Saccharomyces cerevisiae*, *Methods Enzymol.* **304**, 663–672 (1999). [doi:10.1016/S0076-6879\(99\)04040-9](https://doi.org/10.1016/S0076-6879(99)04040-9) [Medline](#)

91. J. G. Henikoff, J. A. Belsky, K. Krassovsky, D. M. MacAlpine, S. Henikoff, Epigenome characterization at single base-pair resolution. *Proc. Natl. Acad. Sci. U.S.A.* **108**, 18318–18323 (2011). [doi:10.1073/pnas.1110731108](https://doi.org/10.1073/pnas.1110731108) [Medline](#)
92. J. Serizay, Sequence-dependent activity and compartmentalization of foreign DNA in a eukaryotic nucleus, Version 1.1.0, Zenodo (2024); <https://zenodo.org/records/14037364>.
93. M. Bodmer-Glavas, K. Edler, A. Barberis, RNA polymerase II and III transcription factors can stimulate DNA replication by modifying origin chromatin structures. *Nucleic Acids Res.* **29**, 4570–4580 (2001). [doi:10.1093/nar/29.22.4570](https://doi.org/10.1093/nar/29.22.4570) [Medline](#)
94. D. G. Batrakou, C. A. Müller, R. H. C. Wilson, C. A. Nieduszynski, DNA copy-number measurement of genome replication dynamics by high-throughput sequencing: The sort-seq, sync-seq and MFA-seq family. *Nat. Protoc.* **15**, 1255–1284 (2020). [doi:10.1038/s41596-019-0287-7](https://doi.org/10.1038/s41596-019-0287-7) [Medline](#)
95. A. Koren, S. A. McCarroll, Random replication of the inactive X chromosome. *Genome Res.* **24**, 64–69 (2014). [doi:10.1101/gr.161828.113](https://doi.org/10.1101/gr.161828.113) [Medline](#)
96. C. Michaelis, R. Ciosk, K. Nasmyth, Cohesins: Chromosomal proteins that prevent premature separation of sister chromatids. *Cell* **91**, 35–45 (1997). [doi:10.1016/S0092-8674\(01\)80007-6](https://doi.org/10.1016/S0092-8674(01)80007-6) [Medline](#)
97. D. de Bruin, M. Lanzer, J. V. Ravetch, Characterization of yeast artificial chromosomes from *Plasmodium falciparum*: Construction of a stable, representative library and cloning of telomeric DNA fragments. *Genomics* **14**, 332–339 (1992). [doi:10.1016/S0888-7543\(05\)80223-X](https://doi.org/10.1016/S0888-7543(05)80223-X) [Medline](#)